Four-body calculation of ^{6}He breakup with the Coulomb-corrected eikonal method

D. Baye,[1,2,*] P. Capel,[1,2,†] P. Descouvemont,[2,‡] and Y. Suzuki[3,§]

[1]*Physique Quantique, C.P. 165/82, Université Libre de Bruxelles (ULB), B 1050 Brussels, Belgium*

[2]*Physique Nucléaire Théorique et Physique Mathématique, C.P. 229, Université Libre de Bruxelles (ULB), B 1050 Brussels, Belgium*

[3]*Department of Physics, and Graduate School of Science and Technology, Niigata University, Niigata 950-2181, Japan*

(Received 17 October 2008; published 13 February 2009)

The elastic breakup of a three-body projectile on a target is studied within the eikonal approximation with full account of final-state interactions. Bound and scattering states are calculated in hyperspherical coordinates on a Lagrange mesh. A correction is introduced to avoid the divergence of breakup cross sections due to the Coulomb interaction. The eikonal approximation allows the direct calculation of various cross sections, and in particular multidifferential cross sections can be obtained. The model is applied to the breakup of ^{6}He on ^{208}Pb. The ^{6}He halo nucleus is described within a three-body $\alpha+n+n$ model involving effective αn and nn interactions. The eikonal phase is obtained from optical potentials between α and n, and the target. Around 0.8 MeV, the total breakup cross sections exhibit a narrow 2^+ resonant peak superimposed over a broad bump corresponding to a 1^- resonance. These results suffer from a disagreement with experimental data at 240 MeV/nucleon, where cross sections are much smaller at low energies. The obtained $E1$ strength distribution resembles other theoretical results and reopens a long-standing problem about the existence of a 1^- low-energy resonance in the ^{6}He continuum.

DOI: 10.1103/PhysRevC.79.024607 PACS number(s): 25.60.Gc, 24.10.−i, 21.45.−v, 27.20.+n

I. INTRODUCTION

Breakup reactions are one of the main tools for studying exotic nuclei and, in particular, halo nuclei [1–3]. Halo nuclei present a large spatial extension and can be viewed as made up of a normal nucleus, the core, and one or two weakly bound nucleons located on the average at large distances, the halo. The short lifetime and fragility of these systems require specific methods of study. Breakup reactions of an exotic projectile on a well-known target allow in principle a reconstruction of the properties of the internal wave function of the projectile. Contrary to early expectations, however, the reconstruction procedure is not simple and must rely on an accurate description of the collision mechanism, first-order perturbation treatments being often not valid or not accurate enough.

Several accurate methods have been developed for the description of breakup reactions (see Ref. [4] for a review): eikonal model [5,6], continuum-discretized coupled channels (CDCC) approximation [7,8], numerical resolution of a three-dimensional time-dependent Schrödinger equation [9–13], and more recently dynamical eikonal approximation [14,15]. They differ by their domain of validity and by their complexity. All these methods have been applied to the breakup of various one-nucleon halo nuclei such as ^{11}Be or ^{8}B. However, they have not been applied yet to the breakup of two-neutron halo nuclei, such as ^{6}He, treated as three-body systems (some calculations assume a two-body core+dineutron structure). Encouraging preliminary steps have been performed with CDCC, but published results are to date restricted to the study of the effect of the inclusion of breakup channels on elastic scattering [16–18]. For three-body projectiles, the time-dependent Schrödinger equation and the dynamical eikonal approximation, which is based on the resolution of the same equation but takes interference effects between different trajectories into account, are presently numerically too heavy. On the contrary, the relative simplicity of the eikonal approximation does allow the four-body study of the breakup of a three-body projectile at intermediate or high energies. This approximation takes account of the interaction at all orders, but it suffered until recently from a serious drawback in the presence of a Coulomb interaction: a divergence due to a wrong asymptotic behavior of the breakup probability at large impact parameters. The divergence was usually eliminated by a cutoff which introduced some arbitrariness in the model.

The adiabatic or sudden approximation made in the usual eikonal model, which consists of neglecting excitations of the projectile, is responsible for that divergence. It indeed assumes a very brief collision time, which is incompatible with the infinite range of the Coulomb interaction. The fact that the adiabatic assumption is responsible for the failure of the eikonal approximation is proved by comparison with the nondivergent dynamical eikonal approximation where this approximation is not performed. A correction to that problem has been proposed by Margueron, Bonaccorso, and Brink [19] and developed by Abu-Ibrahim and Suzuki [20]. The basic idea of this Coulomb-corrected eikonal model is to replace the diverging Coulomb eikonal phase at first order by the corresponding first order of the perturbation theory [21]. The latter, being obtained without adiabatic approximation, does not diverge.

This improved eikonal approximation, the Coulomb-corrected eikonal approximation (CCE), has recently been tested in a comparison with the dynamical eikonal approximation (DEA) for the breakup of ^{11}Be on ^{208}Pb and ^{12}C [22]. The agreement was found to be very good except in

*dbaye@ulb.ac.be
†pierre.capel@centraliens.net
‡pdesc@ulb.ac.be
§suzuki@nt.sc.niigata-u.ac.jp

some observables when the nuclear interaction dominates and dynamical effects are important. The CCE can be considered as a fair, much simpler, approximation of the DEA. The aim of the present paper is to extend eikonal calculations to the breakup of two-neutron halo nuclei and to present a first application with ^{6}He.

The breakup of ^{6}He on lead is interesting, because the α core has a simple structure and experimental data exist [23–25]. In an $\alpha+n+n$ model, it has been considered by several authors within a nondynamical description [26–30]. Those models are based on a calculation of the $E1$ strength distribution. This distribution is multiplied by an equivalent photon number to derive the cross sections. Electric dipole strength distributions are calculated with three-body models in Refs. [26–28]. In Ref. [26], the adiabatic expansion in hyperspherical coordinates is employed. In Ref. [27], the three-body wave function is expanded in hyperspherical harmonics. In both cases, continuum wave functions taking account of final-state interactions are employed. In Ref. [28], the complex rotation method is used to discretize the continuum. Other models of this breakup use either plane waves [29] as final states or a continuum discretized in a box [30].

Dynamical effects are partly included within the distorted-wave impulse approximation in Refs. [31–33]. In that method, the final-state wave function is approximated by the product of a projectile continuum wave function and a distorted wave describing the relative motion of the projectile and the target. Different types of cross sections and the role of correlations are studied in these works.

In the present paper, the Coulomb-corrected eikonal approximation is developed for the three-body breakup of a projectile at intermediate energies within a four-body model. The internal structure of the three-body projectile is described in hyperspherical coordinates, with an expansion in hyperspherical harmonics. This calculation is significantly simplified by the use of the Lagrange-mesh method [34], which was developed for three-body bound states in Ref. [35] and for three-body scattering states in Ref. [36]. The Lagrange-mesh method has the advantage of being accurate with a small number of mesh points. The eikonal model takes approximately into account both nuclear and Coulomb effects, at all orders. Final-state interactions are fully included. The formalism is applied to the elastic breakup of the ^{6}He halo nucleus for which the effective interactions of the α core with the target are well known. The model does not require any optical potential between the ^{6}He projectile and the target. Various breakup cross sections are calculated. Elastic scattering is also studied as a simpler particular case. A different four-body eikonal approach to elastic scattering can be found in Refs. [37,38]. The eikonal model has been shown in Ref. [39] to describe the elastic scattering of halo nuclei in a way as satisfactory as with CDCC [16].

In Sec. II, the derivation of the bound and continuum states of a three-body system composed of a core and two neutrons is described. Scattering states with given final momenta between the projectile constituents are constructed. The expression of the $E1$ strength distribution is established. In Sec. III, the breakup and elastic transition matrix elements are derived within the CCE. The expressions of various cross sections are given. Results are presented and compared with experiment and with other theoretical works in Sec. IV. Concluding remarks are made in Sec. V.

II. BOUND AND CONTINUUM STATES OF A THREE-BODY PROJECTILE

A. Bound and scattering partial waves in hyperspherical coordinates

Let us consider a system of three particles, the core with coordinate $\boldsymbol{r}_c$, charge $Z_c e$, and mass A_c in units of the neutron mass m_n and two neutrons with coordinates $\boldsymbol{r}_1$ and $\boldsymbol{r}_2$. The total mass is $A = A_c + 2$. We start from the Jacobi coordinates $\boldsymbol{r}_{21} = \boldsymbol{r}_2 - \boldsymbol{r}_1$ of neutron 2 with respect to neutron 1 and $\boldsymbol{r}_{c(12)} = \boldsymbol{r}_c - \frac{1}{2}(\boldsymbol{r}_1 + \boldsymbol{r}_2)$ of the core with respect to the center of mass of the neutrons. After removal of the center-of-mass motion, the three-body Hamiltonian of this system can be written as

$$H_0 = -\frac{\hbar^2}{2m_n}(\Delta_x + \Delta_y) + V_{c1} + V_{c2} + V_{12}, \qquad (1)$$

where scaled Jacobi coordinates are defined as $\boldsymbol{x} = \frac{1}{\sqrt{2}}\boldsymbol{r}_{21}$ and $\boldsymbol{y} = \sqrt{\frac{2A_c}{A}}\boldsymbol{r}_{c(12)}$ (see Fig. 1), and V_{ij} is an effective potential between particles i and j ($i, j = c, 1, 2$) [35]. To investigate the breakup cross sections for this system, we need wave functions of such a projectile at both positive and negative energies.

The hyperspherical-harmonics method is an efficient tool for dealing with three-body systems. This formalism is well known (see Refs. [3,35] for details). In the notation of Refs. [35,40], the hyperradius ρ and hyperangle α are defined as $\rho^2 = x^2 + y^2$ and $\alpha = \arctan(y/x)$. The hyperangle α and the orientations Ω_x and Ω_y of $\boldsymbol{x}$ and $\boldsymbol{y}$ provide a set of five angles $\Omega_{5\rho}$. The volume element is $d\boldsymbol{x}\, d\boldsymbol{y} = \rho^5\, d\rho\, d\Omega_{5\rho}$ with $d\Omega_{5\rho} = \sin^2\alpha \cos^2\alpha\, d\alpha\, d\Omega_x\, d\Omega_y$.

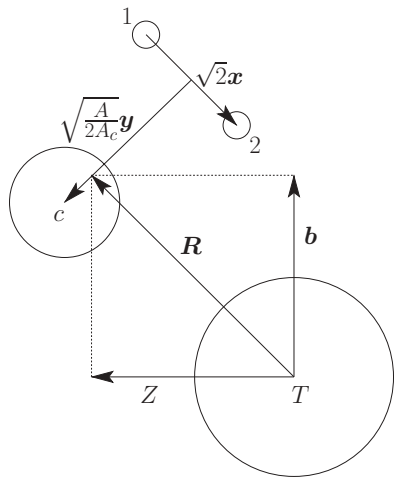

FIG. 1. Scaled internal Jacobi coordinates $\boldsymbol{x}$ and $\boldsymbol{y}$ of the projectile, and transverse and longitudinal components $\boldsymbol{b}$ and Z of the projectile-target coordinate $\boldsymbol{R}$.

A partial wave function $\Psi^{JM\pi}$ is a solution of the Schrödinger equation associated with the three-body Hamiltonian (1) at energy E. It can be expanded as

$$\Psi^{JM\pi}(\rho,\Omega_{5\rho}) = \rho^{-5/2}\sum_{\gamma K}\chi^{J\pi}_{\gamma K}(\rho)\mathcal{Y}^{JM}_{\gamma K}(\Omega_{5\rho}), \qquad (2)$$

where K is the hypermomentum quantum number, index γ stands for (l_x,l_y,L,S), and $\mathcal{Y}^{JM}_{\gamma K}(\Omega_{5\rho})$ are hyperspherical harmonics [35]. The hyperradial wave functions $\chi^{J\pi}_{\gamma K}(\rho)$ are unknown. The parity $\pi = (-1)^K$ of the three-body relative motion restricts the sum over K to even or odd values. Rigorously, the summation over γK should contain an infinite number of terms. In practice, this expansion is limited by a maximum K value, denoted as $K_{\max}$. All l_x and l_y values compatible with $K_{\max}$ (i.e., $l_x + l_y \leqslant K_{\max}$) are included. For weakly bound and scattering states, it is well known that the convergence is rather slow and that large $K_{\max}$ values must be used. The functions $\chi^{J\pi}_{\gamma K}(\rho)$ are derived from a set of coupled differential equations [35,36]. For bound states, approximate solutions can be obtained with an expansion on a square integrable finite basis. However, using the same basis for scattering states raises problems, since they do not vanish at infinity. Their asymptotic form requires a proper treatment. This is made possible within the R-matrix theory [41].

The R-matrix method allows us to match a variational function over a finite interval with the correct asymptotic solutions of the Schrödinger equation. It is based on a division of the configuration space into two regions: an internal region, with hyperradius a, where the solution of the system of coupled equations is given by some variational expansion, and an external region where asymptotic expressions can be used. In the external region, it is assumed that only the Coulomb and centrifugal potentials do not vanish so that the exact solutions are known. For three-body systems, an intermediate region where the potential is not fully negligible is also useful to avoid using a very large internal region [36].

In the following, we assume that the channel radius a is large enough so that the matrix elements necessary in the reaction calculation are well approximated by integrals over the internal region only. In other words, because of the exponential decrease of the bound state entering the transition matrix elements, only the internal part of the scattering state is needed for the reaction. Of course, the *derivation* of the scattering state requires that it be considered over the full configuration space. With this assumption (valid for a values to be adapted to each practical calculation), both bound and scattering hyperradial wave functions are approximated over the internal region by the expansion

$$\chi^{J\pi}_{\gamma K}(\rho) = \sum_{i=1}^{N} c^{J\pi}_{\gamma K i}u_i(\rho), \qquad (3)$$

where the N orthonormal functions $u_i(\rho)$ represent a square-integrable variational basis over $[0,a]$ and $c^{J\pi}_{\gamma K i}$ are the corresponding coefficients.

For the basis functions $u_i(\rho)$, we use the Lagrange-mesh method which is quite efficient for describing two-body bound and scattering states [34,42,43]. This method was extended to three-body bound states in Ref. [35] and to three-body scattering states in Ref. [36]. The N basis functions $u_i(\rho)$ are defined in Eq. (26) of Ref. [44] and in Eq. (42) of Ref. [36]. The mesh points $ax_i \in [0,a]$ are obtained from the zeros of a shifted Legendre polynomial given by $P_N(2x_i - 1) = 0$. The basis functions vanish at the origin and satisfy the Lagrange conditions $u_i(ax_j) = (a\lambda_i)^{-1/2}\delta_{ij}$, i.e., they vanish at all mesh points but one. The main advantage of the Lagrange-mesh technique is to strongly simplify the calculation of matrix elements without loss of accuracy if the Gauss approximation consistent with the mesh is used [35]. Integration over ρ then provides a diagonal potential matrix with matrix elements obtained by a single evaluation of the potential at each mesh point. We refer the reader to Ref. [36] for details.

In a reaction, it is convenient to have similar expansions for the bound and scattering states. The same mesh must thus be used for all states. To this end, the shifted Lagrange-Legendre mesh necessary for describing scattering states with the R-matrix method replaces the Lagrange-Laguerre mesh employed for bound states in Ref. [35]. Hence integrations over the hyperradial coordinate reduce to weighted sums over the mesh points [see Eq. (38) below].

For bound states ($E < 0$), the external wave function decreases exponentially and becomes negligible beyond the internal region. The normalization imposes

$$\sum_{\gamma K}\sum_{i=1}^{N}\left(c^{J\pi}_{\gamma K i}\right)^2 = 1, \qquad (4)$$

since the coefficients are then real.

The normalization of the scattering states ($E > 0$) is fixed by choosing their asymptotic form. Several choices are possible and would lead to apparently different expressions for matrix elements. In any case, the asymptotic behavior of a given partial wave depends on the collision matrix. For real interactions, the collision matrix $\boldsymbol{U}^{J\pi}$ of each partial wave $J\pi$ is unitary and symmetric. For three-body scattering, it differs from two-body collision matrices in an important aspect. Its dimension is not given by the number of open channels but is infinite, since the particles can share the angular momentum in an infinite number of ways. In practical calculations, its dimension depends on the number of hypermomenta included in the calculation, i.e., on the truncation value $K_{\max}$. The entrance channel (labeled below with subscript ω) thus also contains the same number of components.

The asymptotic form of the scattering states with the normalization chosen here is given by

$$\chi^{J\pi}_{\gamma K(\gamma_\omega K_\omega)}(\rho) \underset{\rho\to\infty}{\to} i^{K_\omega+1}(2\pi/k)^{5/2}\left[H^-_{K+2}(k\rho)\delta_{\gamma\gamma_\omega}\delta_{KK_\omega} - U^{J\pi}_{\gamma K,\gamma_\omega K_\omega}H^+_{K+2}(k\rho)\right], \qquad (5)$$

where $k = \sqrt{2m_nE/\hbar^2}$ is the wave number [27,36,45]. The ingoing and outgoing functions read $H^{\pm}_K(x) = \pm i(\pi x/2)^{1/2}[J_K(x) \pm iY_K(x),]$ where $J_K(x)$ and $Y_K(x)$ are Bessel functions of first and second kind, respectively [46]. The indices $\gamma_\omega K_\omega$ denote the partial entrance channel for this solution. The asymptotic behavior (5) fixes in Eq. (3) the normalization of the coefficients $c^{J\pi}_{\gamma K(\gamma_\omega K_\omega)i}$ for scattering states with a given entrance channel.

B. Ingoing and outgoing scattering states

To calculate breakup cross sections, one needs to define outgoing scattering states, i.e., scattering states corresponding to fixed values of the final relative momenta of the three particles. Such states are constructed by time-reversing ingoing scattering states corresponding to fixed values of the initial relative momenta. Before defining them, we first need to consider three-body plane waves.

A six-dimensional plane wave can be expanded as [40]

$$(2\pi)^{-3}\exp[i(\boldsymbol{k}_x\cdot\boldsymbol{x}+\boldsymbol{k}_y\cdot\boldsymbol{y})] = (k\rho)^{-2}\sum_{l_xl_yLM_LK} i^K J_{K+2}(k\rho)\mathcal{Y}^{LM_L*}_{l_xl_yK}(\Omega_{5k})\mathcal{Y}^{LM_L}_{l_xl_yK}(\Omega_{5\rho}), \tag{6}$$

where $k=\sqrt{k_x^2+k_y^2}$ and $\Omega_{5k}=(\Omega_{k_x},\Omega_{k_y},\alpha_k)$ represents five angles corresponding to the directions of $\boldsymbol{k}_x$ and $\boldsymbol{k}_y$ and to $\alpha_k=\arctan(k_y/k_x)$. For a spin state χ^{Sv}, the plane wave with spin is represented as

$$\begin{aligned}(2\pi)^{-3}&\exp[i(\boldsymbol{k}_x\cdot\boldsymbol{x}+\boldsymbol{k}_y\cdot\boldsymbol{y})]\chi^{Sv}\\ &=(2\pi)^{-1/2}(k\rho)^{-5/2}\sum_{\gamma KM_L} i^{K+1}\mathcal{Y}^{LM_L*}_{l_xl_yK}(\Omega_{5k})\\ &\quad\times\sum_J(LSM_Lv|JM)\mathcal{Y}^{JM}_{\gamma K}(\Omega_{5\rho})[H^-_{K+2}(k\rho)-H^+_{K+2}(k\rho)],\end{aligned} \tag{7}$$

where ingoing and outgoing waves are explicitly displayed.

With the asymptotic behavior (5) of the hyperradial partial waves, stationary scattering states are given by [47]

$$\Psi^{(+)}_{\boldsymbol{k}_x\boldsymbol{k}_yS\nu}=(2\pi)^{-3}\rho^{-5/2}\sum_{JM}\sum_{l'_xl'_yL'K'}(L'S'M'_Lv|JM)\mathcal{Y}^{L'M'_L*}_{l'_xl'_yK'}(\Omega_{5k})\times\sum_{\gamma K}\mathcal{Y}^{JM}_{\gamma K}(\Omega_{5\rho})\chi^{J\pi}_{\gamma K(\gamma'K')}(\rho). \tag{8}$$

Their incoming wave is given by the incoming wave in Eq. (7) with the same normalization factor fixed by

$$\left\langle\Psi^{(+)}_{\boldsymbol{k}_x\boldsymbol{k}_yS\nu}\middle|\Psi^{(+)}_{\boldsymbol{k}'_x,\boldsymbol{k}'_yS'\nu'}\right\rangle=\delta(\boldsymbol{k}_x-\boldsymbol{k}'_x)\delta(\boldsymbol{k}_y-\boldsymbol{k}'_y)\delta_{SS'}\delta_{\nu\nu'}. \tag{9}$$

Here and in the following, the Dirac bracket notation represents a six-dimensional integral over the scaled Jacobi coordinates or, equivalently, over the hyperspherical coordinates.

The time-reversed ingoing stationary scattering state

$$\Psi^{(-)}_{\boldsymbol{k}_x\boldsymbol{k}_yS\nu}=(-1)^{S+\nu}\mathcal{K}\Psi^{(+)}_{-k_x,-k_yS-\nu}, \tag{10}$$

where $\mathcal{K}$ is the time-reversal operator, is given after rearrangement by

$$\Psi^{(-)}_{\boldsymbol{k}_x\boldsymbol{k}_yS\nu}=(2\pi)^{-3}\rho^{-5/2}\sum_{JM}\sum_{l'_xl'_yL'K'}(L'S'M'_Lv|JM)\mathcal{Y}^{L'M'_L*}_{l'_xl'_yK'}(\Omega_{5k})\times\sum_{\gamma K}(-1)^K\mathcal{Y}^{JM}_{\gamma K}(\Omega_{5\rho})\chi^{J\pi*}_{\gamma K(\gamma'K')}(\rho). \tag{11}$$

From now on, for simplicity, we write $\mathcal{Y}^{LM_L}_{l_xl_yK}(\Omega_{5k})$ as $\mathcal{Y}^{LM_L}_{\gamma K}(\Omega_{5k})$ even though no spin appears in this case.

C. Dipole strength distribution

The $E1$ strength distribution for transitions from the ground state to the continuum is a property of the projectile that can be extracted from breakup experiments under some simplifying assumptions which will be discussed in Sec. IV. In the hyperspherical coordinate system, the effective $E1$ operator reads

$$\mathcal{M}^{E1}_\mu=eZ_c\left(\frac{2}{A_cA}\right)^{1/2}yY^\mu_1(\Omega_y). \tag{12}$$

The $E1$ transition strength from the ground state at negative energy E_0 with quantum numbers $J_0M_0\pi_0$ to the continuum is defined as

$$\frac{dB(E1)}{dE}=\frac{1}{2J_0+1}\sum_{S\nu M_0\mu}\int d\boldsymbol{k}_xd\boldsymbol{k}_y\delta\left[E-\frac{\hbar^2}{2m_n}\left(k_x^2+k_y^2\right)\right]\times\left|\left\langle\Psi^{(-)}_{\boldsymbol{k}_x\boldsymbol{k}_yS\nu}\middle|\mathcal{M}^{(E1)}_\mu\middle|\Psi^{J_0M_0\pi_0}\right\rangle\right|^2, \tag{13}$$

where E is the excitation energy with respect to the three-particle threshold. With the present definitions, its explicit expression is given by

$$\begin{aligned}\frac{dB(E1)}{dE}=(2\pi)^{-5}&\frac{2Z_c^2e^2}{A_cA}\left(\frac{2m_n}{\hbar^2}\right)^3E^2\sum_{\gamma_\omega K_\omega J}\frac{2J+1}{2J_0+1}\\ &\times\left|\sum_{\gamma K}(-1)^K\sum_{\gamma_0K_0}C^{J_0J1}_{\gamma_0\gamma01}\right.\\ &\times\int_0^{\pi/2}\sin^3\alpha\cos^2\alpha\,\phi^\gamma_K(\alpha)\phi^{\gamma_0}_{K_0}(\alpha)\,d\alpha\\ &\times\left.\int_0^\infty\chi^{J\pi}_{\gamma K(\gamma_\omega K_\omega)}(\rho)\rho\chi^{J_0\pi_0}_{\gamma_0K_0}(\rho)\,d\rho\right|^2,\end{aligned} \tag{14}$$

where $\chi^{J_0\pi_0}_{\gamma_0K_0}$ corresponds to the ground state and $C^{J_0J1}_{\gamma_0\gamma01}$ is a particular case of a general coefficient defined below in Eq. (36). Function $\phi^\gamma_K(\alpha)$ is given by Eq. (9) of Ref. [35].

III. EIKONAL APPROXIMATION FOR A FOUR-BODY SYSTEM

A. Principle

We consider a collision between a three-body projectile and a structureless target with mass A_Tm_n and charge Z_Te. The breakup reaction is described by the four-body Schrödinger equation

$$\left(-\frac{\hbar^2}{2\mu_{PT}}\Delta_R+H_0+V_{PT}(\boldsymbol{R},\boldsymbol{x},\boldsymbol{y})\right)\Phi(\boldsymbol{R},\boldsymbol{x},\boldsymbol{y})=E_T\Phi(\boldsymbol{R},\boldsymbol{x},\boldsymbol{y}), \tag{15}$$

where $\boldsymbol{R}$ is the relative coordinate between the center of mass of the projectile and the target, μ_{PT} is the projectile-target reduced mass, H_0 is given by Eq. (1), and E_T is the total energy of the four-body system. The effective potential between

projectile and target is defined as (see Fig. 1)

$$V_{PT}(\boldsymbol{R},\boldsymbol{x},\boldsymbol{y}) = V_{cT}\left(\boldsymbol{R}+\sqrt{\frac{2}{AA_c}}\,\boldsymbol{y}\right) + V_{1T}\left(\boldsymbol{R}-\sqrt{\frac{A_c}{2A}}\,\boldsymbol{y}-\frac{1}{\sqrt{2}}\boldsymbol{x}\right) + V_{2T}\left(\boldsymbol{R}-\sqrt{\frac{A_c}{2A}}\,\boldsymbol{y}+\frac{1}{\sqrt{2}}\boldsymbol{x}\right). \quad (16)$$

In this expression, each interaction V_{iT} between a constituent of the projectile and the target is simulated by a complex optical potential (including a point-sphere Coulomb interaction for V_{cT}). The projectile is assumed to be initially in its ground state.

In the eikonal approximation, the wave function is factorized as

$$\Phi(\boldsymbol{R},\boldsymbol{x},\boldsymbol{y}) = e^{iKZ}\hat{\Phi}(\boldsymbol{R},\boldsymbol{x},\boldsymbol{y}), \quad (17)$$

where Z is the longitudinal component of $\boldsymbol{R}$, i.e., the component along the direction of the initial wave vector $\boldsymbol{K}$ of the projectile-target relative motion (see Fig. 1). We denote the transverse component of $\boldsymbol{R}$ as $\boldsymbol{b}$ and use $\boldsymbol{R}$ and $(\boldsymbol{b}, Z)$ as equivalent notation. The initial wave number K is related to the total energy by

$$E_T = \frac{\hbar^2K^2}{2\mu_{PT}} + E_0. \quad (18)$$

The Schrödinger equation becomes

$$\left(-\frac{\hbar^2}{2\mu_{PT}}\Delta_R - i\hbar v\frac{\partial}{\partial Z} + H_0 + V_{PT}(\boldsymbol{R},\boldsymbol{x},\boldsymbol{y}) - E_0\right)\hat{\Phi}(\boldsymbol{R},\boldsymbol{x},\boldsymbol{y}) = 0, \quad (19)$$

where $v = \hbar K/\mu_{PT}$ is the initial relative velocity. At high energy, one can assume that $|\Delta_R\hat{\Phi}| \ll K|\partial\hat{\Phi}/\partial Z|$ and neglect the first term. Moreover, the adiabatic approximation consists in replacing H_0 by E_0, i.e., in assuming that the collision time is short enough so that the excitation energy of the projectile can be neglected when compared with the incident energy. The adiabatic approximation is not used in the dynamical eikonal approximation [14,15], but this approach would presently require excessive computation times with a three-body projectile. Then one obtains the approximate eikonal wave function

$$\hat{\Phi}_{\text{eik.}}(\boldsymbol{R},\boldsymbol{x},\boldsymbol{y}) = \exp\left[-\frac{i}{\hbar v}\int_{-\infty}^{Z} V_{PT}(\boldsymbol{b},Z',\boldsymbol{x},\boldsymbol{y})dZ'\right] \times \Psi^{J_0M_0\pi_0}(\boldsymbol{x},\boldsymbol{y}) \quad (20)$$

such that wave function (17) satisfies the initial condition at $Z \to -\infty$, i.e., an incoming Coulomb distorted wave times the ground-state wave function of the projectile (see Ref. [22]). With this wave function, the different scattering properties can be calculated.

B. Transition matrix elements

To obtain cross sections, one must calculate transition matrix elements for the breakup of a two-neutron halo nucleus in its ground state into three fragments. Let $\boldsymbol{k}_c$, $\boldsymbol{k}_1$, $\boldsymbol{k}_2$ be the wave vectors of these fragments in the projectile frame. The relative motions are defined by the relative wave vector of the neutrons

$$\boldsymbol{k}_{21} = \frac{1}{\sqrt{2}}\boldsymbol{k}_x = \frac{1}{2}(\boldsymbol{k}_2 - \boldsymbol{k}_1) \quad (21)$$

and the relative wave vector of the core with respect to the center of mass of the neutrons

$$\boldsymbol{k}_{c(12)} = \sqrt{\frac{2A_c}{A}}\boldsymbol{k}_y = \frac{2}{A}\boldsymbol{k}_c - \frac{A_c}{A}(\boldsymbol{k}_1 + \boldsymbol{k}_2). \quad (22)$$

Here we use the physical wave vectors $\boldsymbol{k}_{21}$ and $\boldsymbol{k}_{c(12)}$ in place of $\boldsymbol{k}_x$ and $\boldsymbol{k}_y$, which are convenient only for calculations in hyperspherical coordinates.

When expressed in coordinates $\boldsymbol{x}$ and $\boldsymbol{y}$, the transition matrix elements read

$$T_{fi} = \left(\frac{A}{A_c}\right)^{3/4}\left\langle e^{i\boldsymbol{K}'\cdot\boldsymbol{R}}\Psi^{(-)}_{\boldsymbol{k}_x\boldsymbol{k}_yS_\nu}(\boldsymbol{x},\boldsymbol{y})|V_{PT}|\Phi(\boldsymbol{R},\boldsymbol{x},\boldsymbol{y})\right\rangle \quad (23)$$

for four-body breakup. The factor $(A/A_c)^{3/4}$ arises from the fact that the integration is performed in coordinates $\boldsymbol{x}$ and $\boldsymbol{y}$ and that the bound-state wave function that we use is normed in this coordinate system [see Eqs. (2)–(4)].

At the eikonal approximation, the exact scattering wave function Φ in Eq. (23) is replaced by its approximation $\Phi_{\text{eik.}}$ given by Eqs. (17) and (20). The transition matrix element can then be written as

$$T_{fi} = i\hbar v\int d\boldsymbol{b}\, e^{-i\boldsymbol{q}\cdot\boldsymbol{b}}S_{S\nu}(\boldsymbol{k}_x,\boldsymbol{k}_y,\boldsymbol{b}). \quad (24)$$

The transferred wave vector is defined as

$$\boldsymbol{q} = \boldsymbol{K}' - \boldsymbol{K}, \quad (25)$$

where $\boldsymbol{K}' = (K', \Omega)$ with $\Omega = (\theta, \varphi)$ is the final relative wave vector of the projectile and target, or equivalently by

$$\boldsymbol{q} = \boldsymbol{k}_c + \boldsymbol{k}_1 + \boldsymbol{k}_2. \quad (26)$$

In the eikonal approximation, vector $\boldsymbol{q}$ is assumed to be orthogonal to the initial wave vector $\boldsymbol{K}$. This approximation also implies that K is large. The final wave number K' of the projectile center of mass verifies

$$E_T = \frac{\hbar^2K'^2}{2\mu_{PT}} + E, \quad (27)$$

with the projectile final excitation energy E. The eikonal breakup amplitudes read

$$S_{S\nu}(\boldsymbol{k}_x,\boldsymbol{k}_y,\boldsymbol{b}) = \left(\frac{A}{A_c}\right)^{3/4}\left\langle\Psi^{(-)}_{\boldsymbol{k}_x\boldsymbol{k}_yS\nu}\middle|e^{i\chi(\boldsymbol{b})}\middle|\Psi^{J_0M_0\pi_0}\right\rangle. \quad (28)$$

In this expression, the final scattering state is given by Eq. (11) and the initial bound state by Eq. (2). In both cases, the hyperradial functions are expanded according to Eq. (3). The eikonal phase shift χ is obtained as

$$\chi = \chi_{cT} + \chi_{1T} + \chi_{2T}. \quad (29)$$

It depends on the transverse part $\boldsymbol{b}$ of $\boldsymbol{R}$ as well as on the transverse parts $\boldsymbol{b}_x$ and $\boldsymbol{b}_y$ of the scaled Jacobi coordinates $\boldsymbol{x}$ and $\boldsymbol{y}$. After a translation of variable Z, the different terms read

$$\chi_{cT}\left(\boldsymbol{b}+\sqrt{\frac{2}{AA_c}}\,\boldsymbol{b}_y\right) = -\frac{1}{\hbar v}\int_{-\infty}^{+\infty} V_{cT}\left(\boldsymbol{b}+\sqrt{\frac{2}{AA_c}}\,\boldsymbol{b}_y, Z'\right) dZ', \qquad (30)$$

and for $j = 1, 2$,

$$\chi_{jT}\left(\boldsymbol{b}-\sqrt{\frac{A_c}{2A}}\,\boldsymbol{b}_y \mp \frac{1}{\sqrt{2}}\boldsymbol{b}_x\right) = -\frac{1}{\hbar v}\int_{-\infty}^{+\infty} V_{jT}\left(\boldsymbol{b}-\sqrt{\frac{A_c}{2A}}\,\boldsymbol{b}_y \mp \frac{1}{\sqrt{2}}\boldsymbol{b}_x, Z'\right) dZ'. \qquad (31)$$

Because of the rotational invariance of the interactions, χ is an even function with respect to the total parity of the four-body system.

Expressions (30) and (31) depend on the orientation of $\boldsymbol{b}$, which appears as a parameter in Eq. (28). To avoid calculating several expressions differing only by the polar angle φ_b, one may write [15]

$$\chi(\boldsymbol{b}) = e^{-i\varphi_b J_{\mathrm{tot},z}}\chi(b\hat{\boldsymbol{x}})\,e^{i\varphi_b J_{\mathrm{tot},z}}, \qquad (32)$$

where $\boldsymbol{J}_{\mathrm{tot}}$ is the total angular momentum of the four-body system. A single calculation per b value is then enough. We choose to perform it with $\boldsymbol{b}$ oriented along the x axis ($\varphi_b = 0$). The eikonal phase factor can be expanded in multipolar components as

$$\exp[i\,\chi(b\hat{\boldsymbol{x}}, \boldsymbol{b}_x, \boldsymbol{b}_y)] = \sum_{\lambda_x\lambda_y\lambda\mu}[Y_{\lambda_x}(\Omega_x)\otimes Y_{\lambda_y}(\Omega_y)]^{\lambda\mu} F^{\lambda\mu}_{\lambda_x\lambda_y}(\alpha,\rho). \qquad (33)$$

The complex functions $F^{\lambda\mu}_{\lambda_x\lambda_y}$ also depend on b. The three indices λ, λ_x, and λ_y satisfy the triangle rule. Different properties are proved in Appendix A. The index λ_x only takes even values because particles 1 and 2 are identical. Hence, with respect to the internal parity operator of the projectile, the parity of the different multipolar components is $(-1)^{\lambda_y}$. For positive (negative) parity, μ is even (odd). If λ is odd, $\mu = 0$ does not exist. The monopole component is purely even, and the dipole component is purely odd. Parity mixing starts at $\lambda = 2$. Functions $F^{\lambda\mu}_{\lambda_x\lambda_y}$ with negative μ values are related to the corresponding functions with positive μ values by a phase factor. Practical aspects of this expansion are discussed in Appendix A.

Introducing the different expansions in the amplitude (28), one obtains

$$S_{S\nu}(\boldsymbol{k_x}, \boldsymbol{k_y}, \boldsymbol{b}) = \left(\frac{A}{A_c}\right)^{3/4}\sum_{JM} e^{i(M_0-M)\varphi_b} \times \sum_{\gamma_\omega K_\omega}(L_\omega SM\,-\nu\nu|JM)\mathcal{Y}^{L_\omega M-\nu}_{\gamma_\omega K_\omega}(\Omega_{5k}) \times \sum_{\lambda\mu}(J_0\lambda M_0\mu|JM)S^{J_0J\lambda\mu}_{\gamma_\omega K_\omega}(E,b), \qquad (34)$$

where partial eikonal breakup amplitudes are defined as

$$S^{J_0J\lambda\mu}_{\gamma_\omega K_\omega}(E,b) = (2\pi)^{-3}\sum_{\gamma K}(-1)^K\sum_{\gamma_0 K_0} \times \sum_{\lambda_x\lambda_y} C^{J_0J\lambda}_{\gamma_0\gamma\lambda_x\lambda_y} I^{J_0J\lambda\mu}_{\gamma_0K_0\gamma K\lambda_x\lambda_y(\gamma_\omega K_\omega)}(E,b). \qquad (35)$$

The rotation operators in Eq. (32) give rise to the phase factor in Eq. (34). The angular momentum coupling coefficients are given by

$$\begin{aligned} C^{J_0J\lambda}_{\gamma_0\gamma\lambda_x\lambda_y} &= \langle l_x l_y LSJ||[Y_{\lambda_x}\otimes Y_{\lambda_y}]^\lambda||l_{x_0}l_{y_0}L_0S_0J_0\rangle \\ &= \frac{1}{4\pi}(-1)^{l_x+l_y+L+S+J_0+\lambda}\delta_{SS_0}\hat{l}_x\hat{l}_y\hat{l}_{x_0}\hat{l}_{y_0}\hat{\lambda}_x\hat{\lambda}_y\hat{\lambda}\hat{L}\hat{L}_0\hat{J}_0 \\ &\quad\times\begin{pmatrix} l_x & \lambda_x & l_{x_0}\\ 0 & 0 & 0\end{pmatrix}\begin{pmatrix} l_y & \lambda_y & l_{y_0}\\ 0 & 0 & 0\end{pmatrix} \\ &\quad\times\begin{Bmatrix} J & J_0 & \lambda\\ L_0 & L & S\end{Bmatrix}\begin{Bmatrix} l_{x_0} & l_{y_0} & L_0\\ \lambda_x & \lambda_y & \lambda\\ l_x & l_y & L\end{Bmatrix}, \end{aligned} \qquad (36)$$

with $\hat{J} = \sqrt{2J+1}$. The remaining double integral over the hyperangle and the hyperradius reads

$$\begin{aligned} I^{J_0J\lambda\mu}_{\gamma_0K_0\gamma K\lambda_x\lambda_y(\gamma_\omega K_\omega)}(E,b) &= \int_0^{\pi/2}\sin^2\alpha\cos^2\alpha\,\phi^\gamma_K(\alpha)\phi^{\gamma_0}_{K_0}(\alpha)\,d\alpha \\ &\quad\times\int_0^\infty \chi^{J\pi}_{\gamma K(\gamma_\omega K_\omega)}(\rho)F^{\lambda\mu}_{\lambda_x\lambda_y}(\alpha,\rho)\chi^{J_0\pi_0}_{\gamma_0K_0}(\rho)\,d\rho. \end{aligned} \qquad (37)$$

Notice that the complex function $\chi^{J\pi}_{\gamma K(\gamma_\omega K_\omega)}$ is not conjugated. With Eq. (3) and the Lagrange conditions, the integral over the hyperradial coordinate is simply obtained at the Gauss approximation as

$$\int_0^\infty \chi^{J\pi}_{\gamma K(\gamma_\omega K_\omega)}(\rho)F^{\lambda\mu}_{\lambda_x\lambda_y}(\alpha,\rho)\chi^{J_0\pi_0}_{\gamma_0K_0}(\rho)d\rho \approx \sum_{i=1}^N c^{J\pi}_{\gamma K(\gamma_\omega K_\omega)i}c^{J_0\pi_0}_{\gamma_0K_0i}F^{\lambda\mu}_{\lambda_x\lambda_y}(\alpha,ax_i). \qquad (38)$$

The transition matrix element (24) can thus be written as

$$T_{fi} = 2\pi i\hbar v \left(\frac{A}{A_c}\right)^{3/4} \sum_{JM\lambda\mu} i^{-|\mu|} e^{-i\mu\varphi} (J_0 \lambda M_0 \mu | JM) \times \sum_{\gamma_\omega K_\omega} (L_\omega S M - \nu\nu | JM) \mathcal{Y}^{L_\omega M-\nu}_{\gamma_\omega K_\omega}(\Omega_{5k}) \times \int_0^\infty J_{|\mu|}(qb) S^{J_0 J\lambda\mu}_{\gamma_\omega K_\omega}(E, b) b\, db \quad (39)$$

after integration over φ_b. The integer index $|\mu| = |M - M_0|$ of the Bessel function $J_{|\mu|}$ is due to the phase factor $e^{i(M_0-M)\varphi_b}$ in Eq. (34).

C. Coulomb-corrected eikonal approximation

The eikonal phase χ can be separated into its Coulomb and nuclear contributions

$$\chi = \chi^N + \chi^C + \chi^C_{PT}. \quad (40)$$

In this expression, χ^C_{PT} is the global elastic Coulomb phase shift between projectile and target. The Coulomb phase shift χ^C due to the tidal Coulomb effects in the projectile is calculated with the bare Coulomb interaction, and the remaining phase shift χ^N contains effects of the nuclear forces as well as of differences between Coulomb forces taking the finite size of the target into account and the bare Coulomb force. At the eikonal approximation, the integral defining χ^C_{PT} diverges and must be calculated with a cutoff [5,6]. Up to an additional cutoff-dependent term that plays no role in the cross sections, it can be written as

$$\chi^C_{PT} = 2\eta \ln(Kb), \quad (41)$$

where $\eta = Z_c Z_T e^2/\hbar v$ is the Sommerfeld parameter. The phase (41) only depends on b.

Because of the long range of the Coulomb force, the Coulomb phase χ^C behaves as $1/b$ at large distances [22]. In the calculation of the breakup cross sections, an integration over $b\,db$ of the $1/b^2$ asymptotic behavior of the squared transition matrix elements diverges logarithmically. This divergence occurs in the first-order term $i\chi^C$ of the expansion of the eikonal Coulomb amplitude $\exp(i\chi^C)$. A plausible correction is therefore to replace in Eq. (28) the factor involving χ^C of the eikonal phase by the expression [19,20]

$$e^{i\chi^C} \to e^{i\chi^C} - i\chi^C + i\chi^{\rm FO}. \quad (42)$$

where $\chi^{\rm FO}$ is the result of first-order perturbation theory, which decreases exponentially at large b. This approximation has been tested and validated for a two-body projectile in Ref. [22]. Explicitly, the tidal Coulomb factor now reads

$$e^{i\chi^C} - i\chi^C + i\chi^{\rm FO} = e^{iQ\hat{\boldsymbol{b}}\cdot\boldsymbol{b}_y} - i[1 - \xi K_1(\xi)] Q\hat{\boldsymbol{b}}\cdot\boldsymbol{b}_y - \xi K_0(\xi) Q z_y, \quad (43)$$

where K_n is a modified Bessel function, z_y is the longitudinal component of $\boldsymbol{y}$,

$$\xi = \frac{(E - E_0)b}{\hbar v}, \quad (44)$$

and

$$Q = \frac{2\eta}{b}\sqrt{\frac{2}{A_c A}}. \quad (45)$$

D. Cross sections

From the transition matrix elements of Eq. (39), various cross sections can be derived. The differential cross section with respect to the eight independent variables reads in the center-of-mass frame

$$\frac{d\sigma}{d\Omega\, d\boldsymbol{k}_{21}\, d\boldsymbol{k}_{c(12)}} = \frac{1}{2J_0+1}\frac{1}{4\pi^2}\left(\frac{\mu_{PT}}{\hbar^2}\right)^2 \frac{K'}{K} \sum_{S\nu M_0} |T_{fi}|^2. \quad (46)$$

The wave numbers k_{21} and $k_{c(12)}$ can be expressed from k and α_k. The total internal energy of the projectile is given by

$$E = \frac{\hbar^2}{2m_n}k^2 = \frac{\hbar^2}{2m_n}\left(k_x^2 + k_y^2\right). \quad (47)$$

Partial integrations lead to various cross sections. The volume element in momentum space becomes

$$d\boldsymbol{k}_{21}\, d\boldsymbol{k}_{c(12)} = \left(\frac{A_c}{A}\right)^{3/2} d\boldsymbol{k}_x\, d\boldsymbol{k}_y = \left(\frac{A_c}{A}\right)^{3/2} k^5 dk\, d\Omega_{5k}, \quad (48)$$

where Ω_{5k} represents the angular parts of $\boldsymbol{k}_{21}$ and $\boldsymbol{k}_{c(12)}$, and α_k. An integration of cross section (46) over the directions Ω, Ω_x, Ω_y of $\boldsymbol{K}'$, $\boldsymbol{k}_{21}$, $\boldsymbol{k}_{c(12)}$ leads to

$$\frac{d\sigma}{dE_{21}dE_{c(12)}} = \frac{\pi}{2(2J_0+1)}\left(\frac{2m_n}{\hbar^2}\right)^2\left(\frac{A}{A_c}\right)^{1/2} k_{21}k_{c(12)} \times \sum_{\gamma_\omega J\lambda\mu} \frac{2J+1}{2\lambda+1}\int_0^\infty \left|\sum_{K_\omega} \phi^{\gamma_\omega}_{K_\omega}(\alpha_k) S^{J_0 J\lambda\mu}_{\gamma_\omega K_\omega}\right|^2 b\, db, \quad (49)$$

where $\phi^{\gamma_\omega}_{K_\omega}$ depends here on α_k, $E_{21} = \hbar^2 k_{21}^2/m_n$, and $E_{c(12)} = A\hbar^2 k^2_{c(12)}/4A_c m_n$. The index γ_ω now represents ($l_{x\omega}$, $l_{y\omega}$, S, L_ω) everywhere. The energies E_{21} and $E_{c(12)}$ correspond to an α + dineutron structure. Cross sections emphasizing a ^{5}He + n structure can be calculated with the same partial amplitudes $S^{J_0 J\lambda\mu}_{\gamma_\omega K_\omega}$ appearing in Eq. (49) [25] (see Appendix B).

Integration of Eq. (46) over Ω_{5k} provides

$$\frac{d\sigma}{d\Omega\, dE} = \frac{1}{2(2J_0+1)}\left(\frac{2m_n}{\hbar^2}\right)^3 E^2 K K' \sum_{\gamma_\omega K_\omega J\lambda\mu} \frac{2J+1}{2\lambda+1} \times \left|\int_0^\infty J_{|\mu|}(qb) S^{J_0 J\lambda\mu}_{\gamma_\omega K_\omega} b\, db\right|^2, \quad (50)$$

with $q \approx 2K\sin(\theta/2)$, since $K' \approx K$. Finally, integrating Eq. (50) over Ω leads to

$$\frac{d\sigma}{dE} = \sum_{J\pi} \frac{d\sigma^{J\pi}}{dE}, \quad (51)$$

where the partial cross sections are given by

$$\frac{d\sigma^{J\pi}}{dE} = \frac{\pi}{2J_0+1}\left(\frac{2m_n}{\hbar^2}\right)^3 E^2 \sum_{\gamma_\omega K_\omega \lambda\mu} \frac{2J+1}{2\lambda+1} \times \int_0^\infty \left|S^{J_0 J\lambda\mu}_{\gamma_\omega K_\omega}\right|^2 b\, db, \quad (52)$$

with K_ω values restricted by $(-1)^{K_\omega} = \pi$.

E. Elastic scattering

Elastic scattering can be studied within the same model. Notice that it only requires core-target and neutron-target optical potentials. There is no need for an additional projectile-target potential. The calculation is much simpler than for breakup as it only involves the ground-state wave function.

The scattering amplitudes are given at the eikonal approximation by

$$f_{M'_0 M_0}(\Omega) = \frac{iK}{2\pi}\int d\boldsymbol{b} e^{-i\boldsymbol{q}\cdot\boldsymbol{b}}\left[\delta_{M'_0 M_0} - S^{J_0}_{M'_0 M_0}(\boldsymbol{b})\right], \quad (53)$$

where the eikonal elastic amplitudes read

$$S^{J_0}_{M'_0 M_0}(\boldsymbol{b}) = \langle \Psi^{J_0 M'_0 \pi_0} | e^{i\chi(\boldsymbol{b})} | \Psi^{J_0 M_0 \pi_0}\rangle. \quad (54)$$

With Eqs. (2), (32), and (33), these amplitudes can be expanded as

$$S^{J_0}_{M'_0 M_0}(\boldsymbol{b}) = e^{-i(M'_0-M_0)\varphi_b}\sum_{\lambda\mu}(J_0\lambda M_0\mu|J_0 M'_0) \times \sum_{\gamma K}\sum_{\gamma_0 K_0}\sum_{\lambda_x\lambda_y} C^{J_0 J_0\lambda}_{\gamma_0\gamma\lambda_x\lambda_y} I^{(0)J_0 J_0\lambda\mu}_{\gamma_0 K_0\gamma K\lambda_x\lambda_y} \quad (55)$$

as a function of the coefficients (36) and of double integrals over the hyperangle and the hyperradius,

$$I^{(0)J_0 J_0\lambda\mu}_{\gamma_0 K_0\gamma K\lambda_x\lambda_y}(b) = \int_0^{\pi/2} \sin^2\alpha\cos^2\alpha\phi^\gamma_K(\alpha)\phi^{\gamma_0}_{K_0}(\alpha)\, d\alpha \times \int_0^\infty \chi^{J_0\pi_0}_{\gamma K}(\rho) F^{\lambda\mu}_{\lambda_x\lambda_y}(\alpha,\rho)\chi^{J_0\pi_0}_{\gamma_0 K_0}(\rho)\, d\rho. \quad (56)$$

The multipole components $F^{\lambda\mu}_{\lambda_x\lambda_y}$ defined in Eq. (33) have here a positive parity (λ_y and μ even).

The treatment of the Coulomb interaction requires some care. As usual, it is convenient to separate the projectile-target Coulomb amplitude to have a faster convergence. The elastic cross section can be written as

$$\frac{d\sigma}{d\Omega} = \frac{1}{2J_0+1}\sum_{M'_0 M_0}\left|f_C(\Omega)\delta_{M'_0 M_0} + \widetilde{f}_{M'_0 M_0}(\Omega)\right|^2, \quad (57)$$

where f_C is the quantal Coulomb scattering amplitude, and the additional scattering amplitudes $\widetilde{f}_{M'_0 M_0}$ are given by

$$\widetilde{f}_{M'_0 M_0}(\Omega) = iK\int_0^\infty J_{|\mu|}(qb)\left[e^{i\chi^C_{PT}(b)}\delta_{M'_0 M_0} - i^{-|\mu|}e^{-i\mu\varphi}S^{J_0}_{M'_0 M_0}(b\hat{\boldsymbol{x}})\right] b\, db, \quad (58)$$

with $\mu = M'_0 - M_0$.

IV. BREAKUP OF THE ^{6}He HALO NUCLEUS

A. Conditions of the ^{6}He calculation

The ^{6}He halo nucleus is described with an α particle as the core. The total intrinsic spin S of the three-body system is thus equal to the total spin of the two halo neutrons. The most complicated ingredient in the calculation is the α+n+n final wave function in the continuum. The conditions of the calculation are thus chosen in such a way that the final state is well described. We closely follow the calculation in Ref. [36]. Another important condition is that the binding energy of ^{6}He be close enough to the experimental value -0.973 MeV [48] in order to have a reasonable extension for the halo.

The α+n+n description ($A_c = 4$) requires αn and nn effective forces. We select the αn potential of Kanada *et al.* [49], which contains central and spin-orbit terms. This potential is deep; i.e., it contains a forbidden state in the $s1/2$ wave which must be eliminated. Except when otherwise mentioned, we perform this elimination with a supersymmetric transformation [50] of the s-wave component, leaving the phase shift unchanged. For the nn potential, we choose the central part of the Minnesota interaction with $u = 1$ [51], which reproduces the deuteron binding energy and the nn scattering length.

The Lagrange-mesh calculation is performed with the shifted Legendre mesh ax_i defined by $P_N(2x_i - 1) = 0$ and the corresponding Gauss quadrature [36,44]. Its definition is fixed by two parameters, the channel radius a and the number of hyperradial mesh points N. Most calculations are performed with $a = 30$ fm and $N = 30$. This choice has been found optimal from comparisons with $(a, N) = (25, 25)$ for which cross sections agree within a few percents, and (30, 35) and (40, 35) for which they agree within much better than 1%.

For the 0^+ ground-state wave function of ^{6}He, we use all partial waves with $K \leqslant K_{\max} = 20$, i.e., 36 spin 0 and 30 spin 1 components. As is well known, the bare αn and nn interactions do not allow the reproduction of the experimental ^{6}He binding energy -0.973 MeV within this three-body model. In Ref. [36], the energy -0.962 MeV is obtained by multiplying the αn interaction by a factor of 1.051. This technique, however, has the drawback of submitting the neutrons to a stronger attraction, which may affect the breakup. Other ways of reproducing this binding energy are employed in the literature. In Ref. [27], an attractive three-body hyperscalar potential, i.e., a central potential depending only on the hyperradius ρ, is added to the different two-body interactions. We have also performed some calculations with this approach. Notice that the hyperscalar potential has no physical relation with realistic three-body interactions. In Ref. [52], the attractive part of the nn Minnesota interaction is increased in the $^1S_0$ partial wave to fit the ^{6}He binding energy. With this technique, only the final-state interaction between the neutrons is slightly affected. We have adopted this approach in the following unless otherwise mentioned. The strength of the longest range Gaussian is increased by a factor of 1.13 giving an energy of -0.986 MeV. The multiplicative factor differs from the factor 1.07 in Ref. [52], because the forbidden state is here eliminated by a supersymmetric transformation whereas it is eliminated in that reference with a pseudopotential [53].

Some calculations with a pseudopotential elimination for the ^{6}He bound state are described below. Let us recall that the pseudopotential elimination cannot be easily applied to continuum states because of the nonlocality of the operator projecting out forbidden states.

In the three-body final scattering state calculated under the same conditions, the three dominant natural-parity partial waves are considered: $J^\pi = 0^+$, 1^-, and 2^+. The number of components grows very fast with J. Hence, we had to adapt $K_{\max}$ (which is even in positive parity and odd in negative parity) to the J value. The values are $K_{\max} = 20$ for 0^+, 19 for 1^-, and 14 for 2^+. The number of components is 66 for 0^+, 155 for 1^-, and 133 for 2^+. These numbers correspond to a single entrance channel $\gamma_\omega K_\omega$, i.e., to a single line in the scattering matrix. However, all possible entrance channels appear in the expressions (49)–(52) of the cross sections. The full number of calculated components is thus given by the square of these values. The corresponding scattering matrices provide many eigenphases. Those with a physical interest are displayed in Fig. 4 of Ref. [36].

B. Conditions of the four-body breakup calculation

The breakup process involves optical potentials between core and target and between neutron and target. We choose the $\alpha + {}^{208}$Pb potential 1 of Bonin *et al.* [54] at 288 MeV for the breakup at 70 MeV/nucleon or 699 MeV for the breakup at 240 MeV/nucleon, and the central part of the $n + {}^{208}$Pb potential of Koning and Delaroche [55] calculated at 70 or 240 MeV.

Different accuracy tests have been performed. The multipole components of the eikonal phase are obtained by a numerical integration. We have checked that the values quoted in Appendix A provide an accuracy of about 0.1%. These multipole components depend on four indices: λ, μ, λ_x, λ_y. The values of λ are fixed by the final angular momentum J, since $J_0^{\pi_0} = 0^+$ for ^{6}He. However, for a given λ, several values of λ_x and λ_y are possible. For $J = 0$–2, we have found that an excellent accuracy is obtained with λ_x and λ_y values that do not exceed 2. Higher values contribute to less than 0.1%.

In Eq. (37), the integration over α is performed with a Gauss-Jacobi quadrature, i.e., with equally spaced mesh points [56]. A high accuracy is obtained with $N_\alpha = 20$ points. The integration over b in the various cross sections is performed with 50 equidistant mesh points separated by 2 fm, up to 100 fm. The accuracy is better than 0.1%. When a Bessel function is present in the integrand [Eq. (50)], additional mesh points corresponding to a smaller step are obtained by interpolation of the eikonal scattering amplitudes $S^{J_0 J \lambda \mu}_{\gamma_\omega K_\omega}$.

The main parameters controlling the accuracy of the calculation concern the expansion of the final ^{6}He scattering state, i.e., $K_{\max}$, and the number of partial waves relevant for the breakup on lead. In the following sections, we discuss the role of these parameters. But let us first discuss the dipole strength, for which J^π is fixed as 1^-.

Except for the choice of the various interactions, which is made on physical grounds, the present model does not contain any adjustable parameter.

C. Electric dipole strength distribution

If nondipole and nuclear transitions are negligible in the breakup process, the cross sections become proportional to the dipole strength. With this assumption, the dipole strength can be extracted from the breakup cross section with [6]

$$\frac{d\sigma}{dE} = \frac{32\pi^2}{9}\left(\frac{Z_T e}{\hbar v}\right)^2 \xi_{\min} K_0(\xi_{\min}) K_1(\xi_{\min}) \frac{dB(E1)}{dE}, \quad (59)$$

where $\xi_{\min}$ depends on a cutoff impact parameter $b_{\min}$ [see Eq. (44)]. Data for the $E1$ strength distribution have been deduced from an ^{6}He breakup experiment on lead at 240 MeV/nucleon [23]. At these high energies, $E1$ transitions are expected to be dominant. The accuracy of this approximation is discussed in Sec. IV E.

We have calculated the $E1$ strength distribution directly with Eq. (14). The sums over K_0 and K must be truncated at some value. For the bound state, the choice is $K_0 \leqslant 20$ as discussed above. For the scattering state, we choose $K \leqslant K_{\max}$. The evolution with respect to $K_{\max}$ is studied in Fig. 2. One observes that the convergence is slow and not fully reached. This is to be expected since the resonance-like structure of the 1^- phase shift presents the same behavior as for 0^+ in Fig. 3 of Ref. [36]. The peak near 1 MeV slowly moves toward lower energies but is almost at the same location for $K_{\max} = 17$ and 19. The present figure is very similar to Fig. 3 of Ref. [27]. The convergence, however, is good enough for a comparison with experimental data involving rather large error bars.

The agreement with the data is good beyond 2 MeV, but they do not exhibit any peak at low energies. The presence of a 1^- resonance is not confirmed. We consider the theoretical bump as due to a resonance, because it corresponds to an increase of the 1^- eigenphase shift similar to that obtained at about the same energy in the 2^+ eigenphase shift (see Fig. 4 of Ref. [36]). Except for the slope of the phase-shift rise, there is no qualitative difference between the behaviors of the eigenphases in these two different partial waves. The three-body model thus suggests the existence of two resonances, the accepted 2^+ resonance and a broader 1^- resonance with a width of about 1 MeV, at low energies in the ^{6}He continuum.

To test the sensitivity to the way the ground-state energy is fitted, the results of various calculations of the $E1$ strength

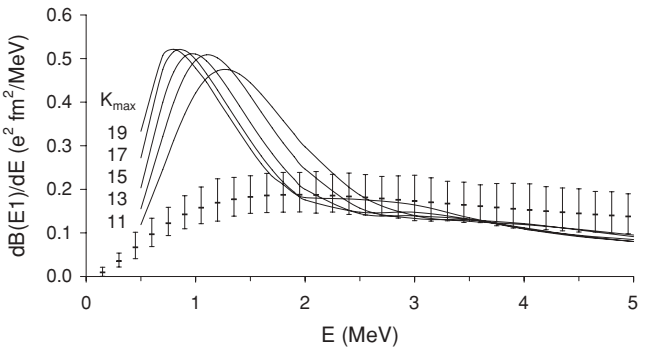

FIG. 2. Convergence of $E1$ strength distribution of ^{6}He with respect to the maximum hypermomentum $K_{\max}$ in the final α+n+n scattering state: comparison of calculations with $K_{\max} = 11$ to 19. Data from Ref. [23].

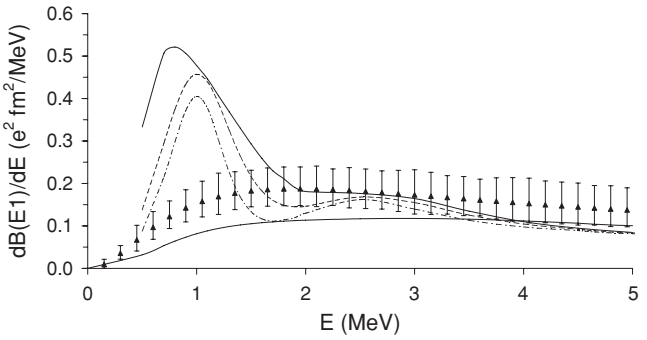

FIG. 3. Comparison of $E1$ strength distributions of ^{6}He calculated for $K_{max} = 19$ with the modified Minnesota interaction (upper solid line), the scaled αn interaction (dash-dotted line), and the three-body hyperscalar potential (dashed line). The lower solid line displays the result with a final plane wave. Data from Ref. [23].

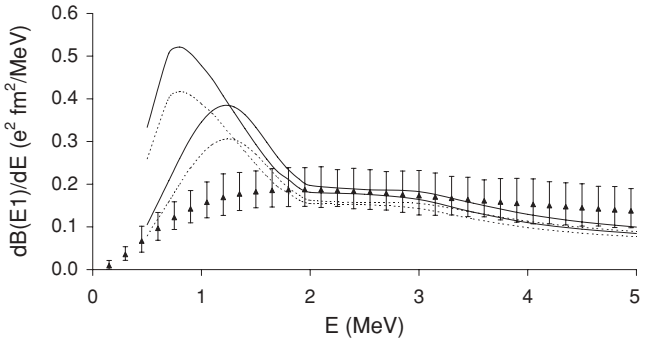

FIG. 4. Comparison of $E1$ strength distributions of ^{6}He calculated for $K_{max} = 19$ with the modified Minnesota interaction (upper solid line, left) and with the unmodified Minnesota interaction for the scattering state (upper solid line, right). Same calculations with a ground-state wave function calculated with the pseudopotential method (dotted lines). Data from Ref. [23].

distribution of ^{6}He are displayed in Fig. 3. The calculation with the modified nn Minnesota interaction is represented by the upper solid line. It corresponds to the $K_{max} = 19$ calculation of Fig. 2. The dash-dotted line represents the result of a calculation with the αn interaction scaled as in Ref. [36]. The resonance peak is a little shifted, and the cross section presents a dip near 1.5 MeV. This dip may be an effect of the stronger core-neutron interaction. A calculation in which the energy is fitted through a three-body hyperscalar potential similar to the one used in Ref. [27] is displayed as a dashed line. In the resonance region, it is very similar to the previous one (dash-dotted line), but the dip is less marked.

We also display in Fig. 3 the $E1$ strength calculated with a plane wave replacing the final scattering state (lower solid line). The convergence with K_{max} is much faster for such calculations. The curve increases smoothly up to 4 MeV. Below 3.5 MeV, the cross section is much smaller than with scattering wave functions and also smaller than experiment. The data thus indicate the occurrence of some effects of final-state interactions even if they do not confirm the existence of a three-body 1^- resonance.

To evaluate the importance of the technique of elimination of the forbidden state, we perform a calculation where the ground-state wave function is calculated with the pseudopotential method [53]. The results are displayed as a dotted line in Fig. 4. One observes that the resonance peak is smaller in that case but remains incompatible with the GSI data. This reduction confirms the results obtained in Ref. [45]. The physical difference between the two techniques of elimination is that supersymmetry eliminates nodes in the wave functions and adds a repulsive core, whereas the pseudopotential moves forbidden states to very high energies but keeps the node structure. Since nodes occur at rather small distances, the difference in the peak height is due to the most internal part of the wave function. From Ref. [45], we can expect some further reduction within a consistent treatment of the scattering state.

The modification of the Minnesota potential performed to fit the ^{6}He binding energy is not necessary for the scattering state. Hence we also display in Fig. 4 the results of calculations performed with the unchanged Minnesota interaction in the final scattering state. Notice that the initial and final states are then obtained with slightly different forces. With this interaction, the resonance is shifted to about 1.2 MeV and broadened. Using the projection technique for the ground state (dotted line) reduces here also the cross section which resembles the one displayed in Fig. 3 of Ref. [27].

The present theoretical behavior is qualitatively common to most previous calculations of the same $E1$ strength taking account of the distortion of the final wave function [26,27]. They also display a peak at low energies, our results being close to those of Ref. [26]. This peak does not appear in some models with a simplified treatment of the continuum. The analytical model of Ref. [29] is based on a final plane wave and on the asymptotic form of the ground-state wave function. The model of Ref. [30] makes use of a discretized continuum. Within models taking final-state interactions into account, an exception can be found in the series of papers [31,32]. Their results do not show any resonance and agree well with the data. The physical origin of this significant difference with respect to earlier works by the same group [27] is not discussed in Refs. [31,32]. A small bump around 4 MeV in their $E1$ strength distribution may indicate that the 1^- resonance still exists but has been pushed to higher energies by the hyperscalar potential and is hence much broadened.

Some three-body models of ^{6}He do not obtain any 1^- resonance [28,57] in spite of a dedicated search. Nevertheless, the $E1$ strength in Ref. [28] exhibits a broad peak very similar to those obtained in the present results without attributing it to a resonance. Although the theoretical situation is not fully clarified, a number of calculations taking full account of final-state interactions predict a broad low-lying 1^- resonance in contradiction with the data of Ref. [23].

The absence of a peak at low energies in the data of Ref. [23] is not contradicted by the experimental results of Ref. [24], but a broad maximum occurs near 2 MeV which can point to a resonant origin. It is at a higher energy than in our results with the unmodified Minnesota interaction in Fig. 4. The situation is reminiscent of the controversy about ^{11}Li breakup. There also the existence of a low-energy peak was uncertain and some contradictions appeared between existing experiments until

the situation was clarified in Ref. [58] and attributed to a lack of sensitivity of previous experiments to the low-energy strength. It would be important to have an experimental confirmation of the existence or nonexistence of a peak at low energies for the ^{6}He breakup.

One should also not forget that the "experimental" $E1$ strength is obtained from cross sections with a number of assumptions. The validity of this approximation can be tested within the present model. This is done in the next sections.

D. Breakup of ^{6}He at 70 MeV/nucleon

In this section, we consider the breakup of ^{6}He on ^{208}Pb at an energy typical of experiments conducted at RIKEN (the Institute of Physical and Chemical Research, Japan). The convergence of the sum in Eq. (51) can be studied by considering separately the cross sections of several partial waves calculated with Eq. (52). Contrary to $E1$ strengths, cross sections are directly measurable. The determination of $E1$ strengths from experiment, such as those displayed in the previous section, rely on different model assumptions. It is assumed that the 1^- partial cross section is dominant and that other contributions are either negligible or can be estimated by some model. It also requires some model assumptions for eliminating nuclear effects. Our aim is to determine the importance of the role of partial waves other than 1^- and to evaluate the role of nuclear forces, first at 70 MeV/nucleon.

The partial and total breakup cross sections are displayed in Fig. 5. The total cross section exhibits a narrow peak at 0.82 MeV superimposed on a broad structure reaching its maximum at about the same energy. The broad maximum is also visible on the $J^\pi = 1^-$ partial cross section. It corresponds to the broad peak in the dipole strength (see Figs. 3 and 4) and to the resonance in the $J^\pi = 1^-$ phase shift appearing in Fig. 4 of Ref. [36].

The narrow peak occurs in the $J^\pi = 2^+$ component and corresponds to a well-known resonance at 0.82 MeV. The conditions of the theoretical calculation are slightly modified for $J^\pi = 2^+$ in order to obtain the correct experimental location of the peak; i.e., we use here a factor of 1.09 in the modified Minnesota interaction. The theoretical width is smaller than the experimental value 0.113 MeV. This resonance should be visible in a breakup experiment on lead if the resolution does not broaden the narrow peak too much and does not make it undetectable. It should be easier to observe in an experiment on a light target [59,60].

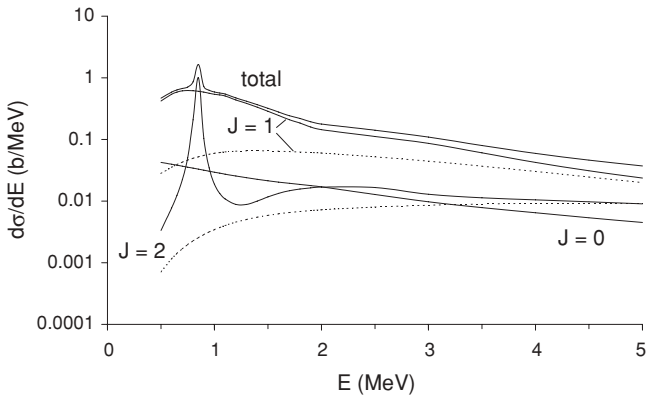

FIG. 5. Eikonal calculation of total and 0^+, 1^-, 2^+ partial cross sections of ^{6}He breakup on ^{208}Pb at 70 MeV/nucleon (solid lines). The dotted lines correspond to final plane waves.

As expected, the 1^- contribution dominates, but the 0^+ and 2^+ contributions are not negligible. Together they range from about 10% at low energies (off resonance) to about 35% at 5 MeV. Below 1 MeV, the 0^+ contribution is much larger than the 2^+ contribution, but they have the same magnitude around 2 MeV, and the 2^+ contribution becomes twice as large as the 0^+ one at 5 MeV. Cross sections leading to unnatural parity states (not shown) are smaller by several orders of magnitude.

Results of calculations with plane waves neglecting final-state interactions are represented as dotted lines. For $J^\pi = 1^-$, the plane-wave cross section is always smaller than the one involving final-state interactions; whereas for 2^+, it becomes similar around 4 MeV. This shows that final-state effects are important, even off resonance.

In Fig. 6, the eikonal partial cross section to the 1^- final state (lower solid line) is compared with approximation (59) based on the $E1$ strength for two values of the cutoff parameter $b_{\min}$. For $b_{\min} = 12$ fm (dashed line), both approximations agree very well at all energies. The total cross section is also represented in Fig. 6 (upper solid curve). Quite logically, it is underestimated.

With the smaller cutoff radius $b_{\min} = 10$ fm (dotted line), the 1^- cross section is overestimated everywhere, but the total cross section is better approximated. If the eikonal total cross section were used to extract the $E1$ strength (off 2^+ resonance), the $E1$ strength would be overestimated for the optimal choice $b_{\min} = 12$ fm but would fortuitously be better for $b_{\min} = 10$ fm. The extraction of the $E1$ strength from data at 70 MeV/nucleon is thus sensitive to two uncertainties, the choice of cutoff radius $b_{\min}$ and the way of correcting for other partial waves than 1^-.

Double-differential cross sections $d\sigma/dE_{21}\,dE_{c(12)}$ [Eq. (49)] provide information about correlations. Such cross sections are displayed for $J^\pi = 1^-$ in the upper part of

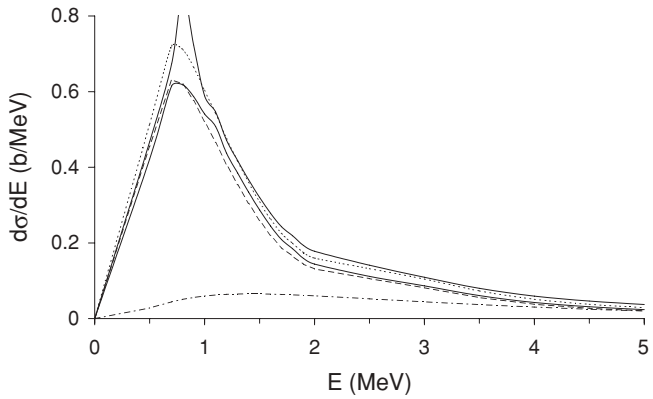

FIG. 6. Comparison of the eikonal calculation of the 1^- partial cross section (lower solid line) with approximation (59) based on the $E1$ strength [Eq. (13)] ($b_{\min} = 10$ fm, dotted line; $b_{\min} = 12$ fm, dashed line) for ^{6}He breakup on ^{208}Pb at 70 MeV/nucleon, and with a calculation involving a final plane wave (dash-dotted line). The upper solid line represents the total cross section.

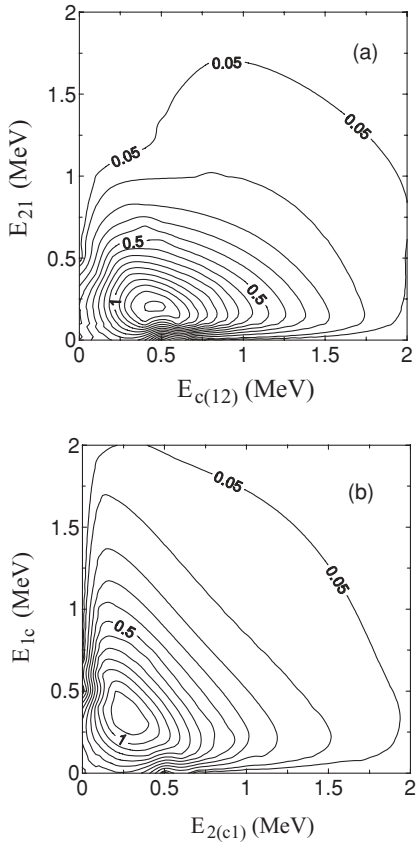

FIG. 7. (a) 1^- component of the double-differential cross sections $d\sigma/dE_{21}\,dE_{c(12)}$ in b/MeV^2 as a function of partial energies E_{21} and $E_{c(12)}$ [Eq. (49)] for ^{6}He breakup on ^{208}Pb at 70 MeV/nucleon. (b) Same for $d\sigma/dE_{1c}dE_{2(c1)}$.

Fig. 7. One observes a pronounced maximum around $E_{c(12)} = 0.5$ MeV and $E_{21} = 0.2$ MeV which corresponds to the broad 1^- resonance that we obtain. This could be interpreted as a slightly dominant α-dineutron character at about 0.5 MeV in the relative motion of the core and the dineutron. This figure is rather similar to Fig. 3 (lower left) of Ref. [33], where a broad 1^- peak is also visible. Since this resonance remains controversial, we do not show the total cross section.

The energies E_{21} and $E_{c(12)}$ occur naturally in the Jacobi coordinate system that we have been using. This can be called the dineutron or T system. Another, completely equivalent, coordinate system involving the relative coordinates between one neutron and the core and between the second neutron and their center of mass would lead to identical results, though in a more complicated way because of the identity of the neutrons. It is called the ^{5}He or Y system. It leads to partial energies E_{1c} and $E_{2(c1)}$. Double-differential cross sections $d\sigma/dE_{1c}\,dE_{2(c1)}$ can, however, be obtained directly from results in the first coordinate system [25] with the help of Raynal-Revai coefficients [40]. This procedure is summarized in Appendix B. The resulting cross sections are displayed in the lower panel of Fig. 7. The resonance now appears as a peak with $E_{1c} \approx E_{2(c1)} \approx 0.4$ MeV. This corresponds to a rather compact structure with both neutrons behaving in a similar way. If the 1^- resonance exists, measurements of these types of cross sections would help clarify its structure. If it does not exist, they may help understand the origin of the wrong theoretical prediction.

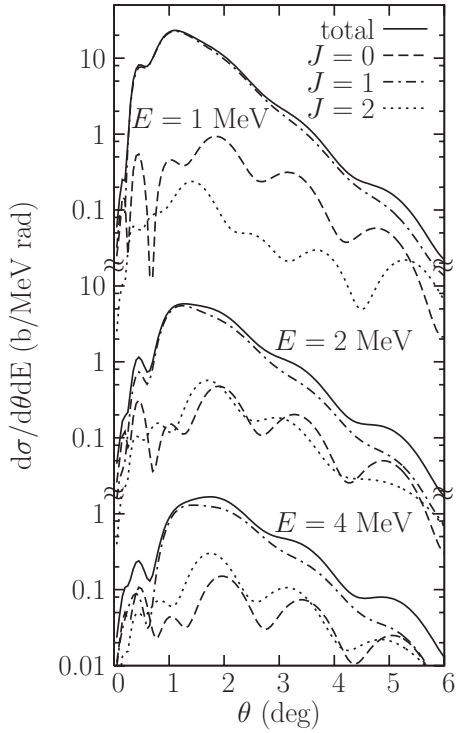

FIG. 8. Double-differential cross sections $d\sigma/d\theta\,dE = 2\pi \sin\theta\, d\sigma/d\Omega\, dE$ (solid lines) as a function of the scattering angle for ^{6}He breakup on ^{208}Pb at 70 MeV/nucleon. Decomposition in partial waves: 0^+ (dashed lines), 1^- (dash-dotted lines), 2^+ (dotted lines).

Another type of double-differential cross sections is interesting, i.e., $d\sigma/d\Omega\, dE$ [Eq. (50)] as a function of the scattering angle θ. They are presented in Fig. 8 with their decomposition in partial waves for three energies. They display rather weak oscillations. At 1 MeV, near the maximum of the 1^- resonance but off the 2^+ resonance, the $J^\pi = 1^-$ component strongly dominates with some contribution of 0^+ near 5°. At 2 MeV, off the 1^- resonance, the other components remain small but are the main origin of the oscillations of the total cross section. From 2 to 4 MeV, one observes an increasing role of the 2^+ partial wave.

E. Breakup of ^{6}He at 240 MeV/nucleon

In this section, we consider the breakup of ^{6}He on ^{208}Pb at the higher energy of the GSI experiments [23,25]. The calculated total and partial cross sections $d\sigma/dE$ are displayed in Fig. 9, which is qualitatively very similar to Fig. 5. The 1^- partial wave dominates somewhat more than at 70 MeV/nucleon, but the 0^+ and 2^+ contributions are far from negligible. The 2^+ resonance is still clearly visible in the total cross section. The 0^+ contribution amounts to about 10% of the total beyond 2 MeV. The 2^+ contribution increases from about 10% to more than 20% between 2 and 5 MeV.

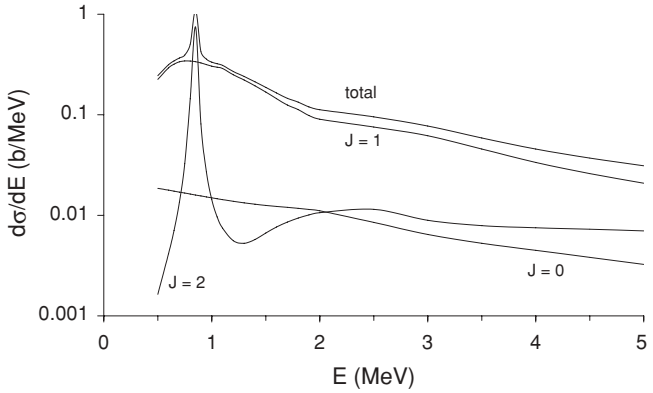

FIG. 9. Eikonal calculation of the total and 0^+, 1^-, 2^+ partial cross sections of ^{6}He breakup on ^{208}Pb at 240 MeV/nucleon.

The total eikonal cross section (solid line) and the 1^- partial cross section (dashed line) at 240 MeV/nucleon are compared with the experimental data of Ref. [23] in Fig. 10. At low energies, the theoretical bump corresponding to the 1^- resonance is not visible in the data. As expected, the disagreement is similar to the one observed in Fig. 3. This means that the problem is not related to the use of the eikonal approximation. When the ground-state wave function is calculated with the projection technique for the αn potential (dotted line) in place of the supersymmetric αn potential (dashed line), the 1^- partial cross section becomes smaller and thus closer to experiment at energies below 2 MeV, but the disagreement still occurs.

A possible 1^- bump should be reinforced by the 2^+ resonance peak (broadened by the experimental resolution). The small bump around 0.8 MeV in the data agrees with the location of the 2^+ resonance but seems to be too weak to agree with its expected properties. Between 2 and 3 MeV, the agreement between theory and experiment becomes quite good (let us recall that there is no free parameter). Beyond 3 MeV, the theory is lower than the data, but this could be attributed to the fact that the experiment does not separate elastic from inelastic breakup.

We make no attempt to compare our results with the angular differential cross section $d\sigma/d\theta$ from Ref. [25], because it would require an integration over the energy E that would be made meaningless by the 1^- resonance problem.

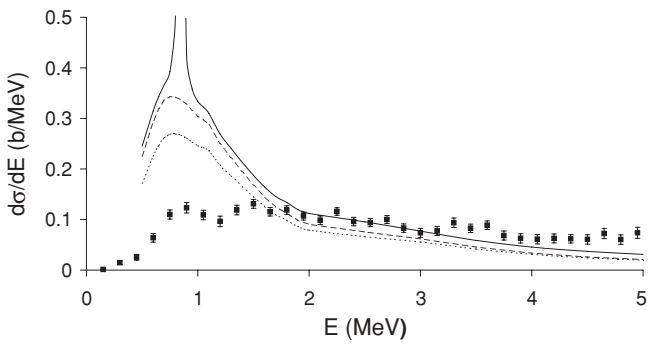

FIG. 10. Comparison between the total eikonal cross section (solid line) and 1^- partial cross sections (supersymmetry, dashed line; projection, dotted line) of ^{6}He breakup on ^{208}Pb at 240 MeV/nucleon with the experimental data of Ref. [23].

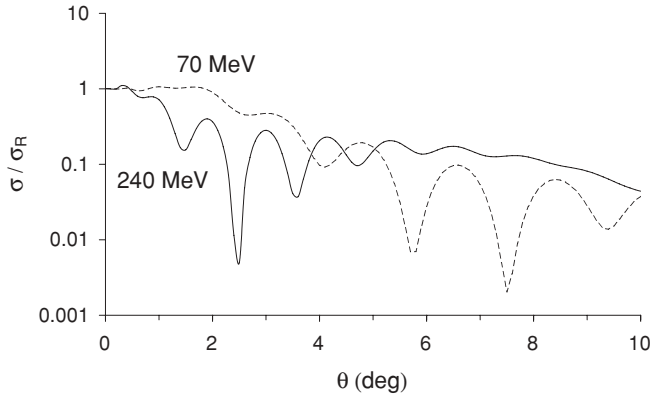

FIG. 11. Ratio to the Rutherford cross section of the elastic cross section of ^{6}He on ^{208}Pb at 70 and 240 MeV/nucleon.

F. Elastic scattering

Elastic scattering can be calculated under the same conditions. The corresponding results at 70 and 240 MeV/nucleon are presented in Fig. 11. Since only αn and nn interactions are involved, the calculation takes full account of the halo structure of the ^{6}He nucleus. Moreover, there is no need for fitting parameters in an ^{6}He-lead potential. On the contrary, inverting the theoretical results would allow deriving such a potential. However, this effort would only be interesting after the theoretical results have been confirmed by experimental data on this elastic scattering.

V. CONCLUSION

In this work, we present a reaction model framework for the study of the elastic breakup of a three-body projectile on some target. The projectile ground and continuum (resonant and nonresonant) states are calculated in hyperspherical coordinates according to the techniques of Refs. [35,36]. The model thus takes full account of final-state interactions. It makes use of the eikonal approximation corrected for Coulomb effects [19,20,22]. This approximation avoids a well-known divergence problem of the Coulomb interaction. The calculation is simplified by the use of the Lagrange-mesh method with which a fair convergence is obtained with a rather small number of hyperradial mesh points. The main limitation on accuracy comes from the truncation with respect to the hypermomentum quantum number K. The model should be valid for light and heavy targets. It can also be used for elastic scattering.

Previous studies involving final-state interactions were either indirect [26–28], i.e., based on first-order perturbation theory and on dipole strengths, or made use of a simpler treatment of the dynamics [31–33]. The advantage of the present eikonal approach is that Coulomb and nuclear effects appear at all orders and that the projectile-target motion is driven by the core-target and neutron-target optical potentials.

As a first application, we consider the elastic breakup of ^{6}He on lead at two energies typical of RIKEN and GSI experiments for which the eikonal approximation is valid. The three-body $\alpha+n+n$ model of ^{6}He involves αn and nn effective forces, not only for the initial bound state but also for the final scattering states. This aspect is important because the results differ much from those based on a final plane wave. In addition to the behavior of the dominant 1^- component, the behaviors of the 0^+ and 2^+ partial cross sections have been determined and can serve as an indicator of the magnitude of inaccuracies in the first-order approach and in the extraction of the $E1$ strength from data.

Since data exist at 240 MeV, a comparison of theory and experiment is possible at that energy. The result reopens a long-standing problem. The theoretical cross sections at 70 and 240 MeV display around 0.8 MeV a narrow peak superimposed on a broader bump. These structures are due to a well known 2^+ resonance and to a broad 1^- resonance, respectively. We consider both of them as resonances, since they appear in a qualitatively similar way as fast increases of the corresponding eigenphase shifts. The GSI data [23] do not show the low-energy bump predicted by the present and several other models describing the effects of final-state interactions. The Michigan State University data [24] are compatible with the existence of a resonance, but its location is significantly higher than suggested by the present theory.

The disagreement is in no way related to the reaction model used, i.e., the eikonal approximation. It is also not related to the optical potentials between α or n and the target. In fact, it indicates a lack of accord of the theoretical description of the ^{6}He continuum with the existing data. If the disagreement is due to theory, it must concern either the interactions between the ^{6}He constituents (which looks rather unlikely) or a problem with the very description of continuum states which would also appear in Refs. [26,27], i.e., in calculations independent from the present one. In any case, the variation of the shape of the broad resonance with the choice of potential and with the type of forbidden-state elimination deserves further investigation.

The existence or nonexistence of a 1^- resonance in the continuum of ^{6}He is an important physical issue which should be clarified by further experiments. If new experimental data confirm that this resonance does not exist, the description of final continuum states in the existing models will be challenged.

We plan to apply the same model to the breakup of the ^{11}Li and ^{14}Be halo nuclei for which data also exist [58,60]. The comparison with experiment may help clarify the origin of the present disagreement.

ACKNOWLEDGMENTS

We thank T. Aumann for sending his data and T. Nakamura for interesting discussions. This work has been done in the framework of the agreement between the Japan Society for the Promotion of Science (JSPS) and the Fund for Scientific Research of Belgium (F.R.S.-FNRS). The authors acknowledge support of the Fonds de la Recherche Scientifique Collective (FRSC). Y.S. acknowledges the support of the Grant for the Promotion of Niigata University Research Projects (2005–2007). P.C. and P.D. acknowledge the support of the F.R.S.-FNRS. This text presents research results of the Belgian program P6/23 on interuniversity attraction poles initiated by the Belgian-state Federal Services for Scientific, Technical and Cultural Affairs (FSTC).

APPENDIX A: MULTIPOLAR COMPONENTS OF EIKONAL PHASE

The multipolar components of the eikonal phase are given by

$$F^{\lambda\mu}_{\lambda_x\lambda_y} = \sum_{\mu_x\mu_y} (\lambda_x\lambda_y\mu_x\mu_y|\lambda\mu) F^{\mu_x\mu_y}_{\lambda_x\lambda_y}, \tag{A1}$$

with

$$F^{\mu_x\mu_y}_{\lambda_x\lambda_y} = \int d\Omega_x \int d\Omega_y Y^{\mu_x *}_{\lambda_x}(\Omega_x) Y^{\mu_y *}_{\lambda_y}(\Omega_y) \exp[i\chi(b\hat{\boldsymbol{x}}, \boldsymbol{b}_x, \boldsymbol{b}_y)]. \tag{A2}$$

We choose vector $\boldsymbol{b}$ in the x direction ($\varphi_b = 0$).

The eikonal shift function χ is invariant under the following symmetry operations:

$$\theta_x \rightarrow \pi - \theta_x, \tag{A3}$$

$$\theta_y \rightarrow \pi - \theta_y, \tag{A4}$$

$$\varphi_x \rightarrow 2\pi - \varphi_x \quad \text{and} \quad \varphi_y \rightarrow 2\pi - \varphi_y, \tag{A5}$$

$$\varphi_x \rightarrow \pi + \varphi_x. \tag{A6}$$

Properties (A3) and (A4) arise from the fact that χ does not depend on the z components of $\boldsymbol{x}$ and $\boldsymbol{y}$. Property (A5) is due to the symmetry of the potentials with respect to the xz plane. Property (A6) is a consequence of the identity of neutrons 1 and 2.

From these properties, one deduces that the $F^{\mu_x\mu_y}_{\lambda_x\lambda_y}$ vanish for λ_x odd, μ_x odd, and $\lambda_y + \mu_y$ odd. These functions have the symmetry property

$$F^{-\mu_x-\mu_y}_{\lambda_x\lambda_y} = (-1)^{\mu_x+\mu_y} F^{\mu_x\mu_y}_{\lambda_x\lambda_y}. \tag{A7}$$

With these symmetry properties, the integration domain in the four-dimensional integral (A2) can be reduced by a factor of 16. For λ_x, μ_x, and $\lambda_y + \mu_y$ even, the simplified integrals explicitly read

$$F^{\mu_x\mu_y}_{\lambda_x\lambda_y} = 16 \int_0^{\pi/2} \sin\theta_x\, d\theta_x \int_0^{\pi/2} \sin\theta_y\, d\theta_y \int_0^{\pi} d\varphi_x \int_0^{\pi} d\varphi_y \times Y^{\mu_x}_{\lambda_x}(\theta_x, 0) Y^{\mu_y}_{\lambda_y}(\theta_y, 0) \cos(\mu_x\varphi_x + \mu_y\varphi_y) \times \exp[i\chi(b\hat{\boldsymbol{x}}, \boldsymbol{b}_x, \boldsymbol{b}_y)]. \tag{A8}$$

The $F^{\lambda\mu}_{\lambda_x\lambda_y}$ vanish for λ_x odd and for $\lambda_y + \mu$ odd. They have the symmetry property

$$F^{\lambda-\mu}_{\lambda_x\lambda_y} = (-1)^{\lambda_x+\lambda_y+\lambda-\mu} F^{\lambda\mu}_{\lambda_x\lambda_y}. \tag{A9}$$

Hence components with $\mu = 0$ vanish if λ is odd.

Unfortunately, these properties do not all apply to $\chi^{\rm FO}$, which requires a separate treatment. Contrary to the invariance (A4), it satisfies

$$\chi^{\rm FO} \underset{\theta_y \to \pi - \theta_y}{\to} -\chi^{\rm FO} \tag{A10}$$

[see the last term in Eq. (43)]. Hence, the components of $e^{i\chi^N}\chi^{\rm FO}$ in the corrected eikonal phase $e^{i\chi}$ vanish for λ_x odd and for $\lambda_y + \mu$ even.

The integration in Eq. (A8) is performed with Gauss quadratures: a Gauss-Legendre quadrature with N_θ points for θ_x and θ_y and a Gauss-Fourier quadrature (i.e., constant spacing and equal weights) with N_φ points for φ_x and φ_y. Typical values are $N_\theta = 12$ and $N_\varphi = 16$. The integration over Z' of the nuclear part in Eqs. (30) and (31) is performed for $Z' > 0$ with $N_Z = 60$ equidistant mesh points with a constant step of 0.5 fm.

APPENDIX B: CHANGE OF OBSERVED WAVE VECTORS

The wave vectors $\boldsymbol{k}_{21}$ and $\boldsymbol{k}_{c(12)}$ correspond to an α + dineutron structure (or T structure). One can equivalently consider the wave vectors corresponding to a ^{5}He + n structure (or Y structure), i.e., the neutron-core wave vector

$$\boldsymbol{k}_{1c} = \frac{1}{A_c + 1}(A_c \boldsymbol{k}_1 - \boldsymbol{k}_c), \tag{B1}$$

and the wave vector for the relative motion of the second neutron with respect to the ^{5}He center of mass

$$\boldsymbol{k}_{2(c1)} = \frac{A_c + 1}{A}\boldsymbol{k}_2 - \frac{1}{A}(\boldsymbol{k}_c + \boldsymbol{k}_1). \tag{B2}$$

Since the Jacobian of the transformation is equal to unity, the cross sections are related by

$$\frac{d\sigma}{d\Omega\, d\boldsymbol{k}_{1c}\, d\boldsymbol{k}_{2(c1)}} = \frac{d\sigma}{d\Omega\, d\boldsymbol{k}_{21}\, d\boldsymbol{k}_{c(12)}}. \tag{B3}$$

However, they must be expressed as a function of the new wave vectors $\boldsymbol{k}_{1c}$ and $\boldsymbol{k}_{2(c1)}$. We briefly summarize the simple procedure described in Ref. [25].

In Eqs. (46) and (39), the dependence on the wave vectors is fully included in the hyperspherical harmonics $\mathcal{Y}^{L_\omega M-\nu}_{\gamma_\omega K_\omega}(\Omega_{5k})$. These T harmonics can be transformed into Y harmonics with the help of the Raynal-Revai coefficients [40],

$$\mathcal{Y}^{L_\omega M}_{l_{x_\omega} l_{y_\omega} K_\omega}(\Omega^{\rm T}_{5k}) = \sum_{l_x l_y} \langle l_x l_y | l_{x_\omega} l_{y_\omega} \rangle_{K_\omega L_\omega} \mathcal{Y}^{L_\omega M}_{l_x l_y K_\omega}(\Omega^{\rm Y}_{5k}). \tag{B4}$$

Hence the expressions of the transition matrix element (39) and of all cross sections of Sec. III D remain valid for $\boldsymbol{k}_{1c}$ and $\boldsymbol{k}_{2(c1)}$ provided that the eikonal amplitudes are understood as the Y amplitudes defined by

$$S^{J_0 J \lambda\mu}_{\gamma_\omega K_\omega}({\rm Y}) = \sum_{l_x l_y} \langle l_{x_\omega} l_{y_\omega} | l_x l_y \rangle_{K_\omega L_\omega} S^{J_0 J \lambda\mu}_{\gamma K_\omega}({\rm T}), \tag{B5}$$

with $\gamma = (l_x, l_y, L_\omega, S)$.

[1] I. Tanihata, J. Phys. G **22**, 157 (1996).
[2] P. G. Hansen, A. S. Jensen, and B. Jonson, Annu. Rev. Nucl. Sci. **45**, 591 (1995).
[3] M. V. Zhukov, B. V. Danilin, D. V. Fedorov, J. M. Bang, I. J. Thompson, and J. S. Vaagen, Phys. Rep. **231**, 151 (1993).
[4] D. Baye, Eur. Phys. J. Special Topics **156**, 93 (2008).
[5] R. J. Glauber, in *High Energy Collision Theory,* Lectures in Theoretical Physics, edited by W. E. Brittin and L. G. Dunham (Interscience, New York, 1959), Vol. 1, p. 315.
[6] Y. Suzuki, R. G. Lovas, K. Yabana, and K. Varga, *Structure and Reactions of Light Exotic Nuclei* (Taylor and Francis, London, 2003).
[7] M. Yahiro, Y. Iseri, H. Kameyama, M. Kamimura, and M. Kawai, Prog. Theor. Phys. Suppl. **89**, 22 (1986).
[8] J. A. Tostevin, F. M. Nunes, and I. J. Thompson, Phys. Rev. C **63**, 024617 (2001).
[9] T. Kido, K. Yabana, and Y. Suzuki, Phys. Rev. C **53**, 2296 (1996).
[10] H. Esbensen, G. F. Bertsch, and C. A. Bertulani, Nucl. Phys. **A581**, 107 (1995).
[11] S. Typel and H. H. Wolter, Z. Naturforsch. Teil A **54**, 63 (1999).
[12] V. S. Melezhik and D. Baye, Phys. Rev. C **59**, 3232 (1999).
[13] P. Capel, D. Baye, and V. S. Melezhik, Phys. Rev. C **68**, 014612 (2003).
[14] D. Baye, P. Capel, and G. Goldstein, Phys. Rev. Lett. **95**, 082502 (2005).
[15] G. Goldstein, D. Baye, and P. Capel, Phys. Rev. C **73**, 024602 (2006).
[16] T. Matsumoto, E. Hiyama, K. Ogata, Y. Iseri, M. Kamimura, S. Chiba, and M. Yahiro, Phys. Rev. C **70**, 061601(R) (2004).
[17] T. Matsumoto, T. Egami, K. Ogata, Y. Iseri, M. Kamimura, and M. Yahiro, Phys. Rev. C **73**, 051602(R) (2006).
[18] M. Rodríguez-Gallardo, J. M. Arias, J. Gómez-Camacho, R. C. Johnson, A. M. Moro, I. J. Thompson, and J. A. Tostevin, Phys. Rev. C **77**, 064609 (2008).
[19] J. Margueron, A. Bonaccorso, and D. M. Brink, Nucl. Phys. **A703**, 105 (2002).
[20] B. Abu-Ibrahim and Y. Suzuki, Prog. Theor. Phys. **112**, 1013 (2004); **114**, 901 (2005).
[21] K. Alder and A. Winther, *Electromagnetic Excitation* (North-Holland, Amsterdam, 1975).
[22] P. Capel, D. Baye, and Y. Suzuki, Phys. Rev. C **78**, 054602 (2008).
[23] T. Aumann, D. Aleksandrov, L. Axelsson, T. Baumann, M. J. G. Borge, L. V. Chulkov, J. Cub, W. Dostal, B. Eberlein, T. W. Elze *et al.*, Phys. Rev. C **59**, 1252 (1999).
[24] J. Wang, A. Galonsky, J. J. Kruse, E. Tryggestad, R. H. White-Stevens, P. D. Zecher, Y. Iwata, K. Ieki, Á. Horváth, F. Deák *et al.*, Phys. Rev. C **65**, 034306 (2002).
[25] L. V. Chulkov, H. Simon, I. J. Thompson, T. Aumann, M. J. G. Borge, T. W. Elze, H. Emling, H. Geissel, L. V. Grigorenko, M. Hellström *et al.*, Nucl. Phys. **A759**, 23 (2005).
[26] A. Cobis, D. V. Fedorov, and A. S. Jensen, Phys. Rev. Lett. **79**, 2411 (1997).
[27] B. V. Danilin, I. J. Thompson, J. S. Vaagen, and M. V. Zhukov, Nucl. Phys. **A632**, 383 (1998).
[28] T. Myo, K. Kato, S. Aoyama, and K. Ikeda, Phys. Rev. C **63**, 054313 (2001).

[29] A. Pushkin, B. Jonson, and M. V. Zhukov, J. Phys. G **22**, L95 (1996).
[30] K. Hagino and H. Sagawa, Phys. Rev. C **76**, 047302 (2007).
[31] S. N. Ershov, B. V. Danilin, and J. S. Vaagen, Phys. Rev. C **64**, 064609(R) (2001).
[32] S. N. Ershov, B. V. Danilin, and J. S. Vaagen, Phys. Rev. C **74**, 014603 (2006).
[33] B. V. Danilin, J. S. Vaagen, T. Rogde, S. N. Ershov, I. J. Thompson, and M. V. Zhukov, Phys. Rev. C **76**, 064612 (2007).
[34] D. Baye and P.-H. Heenen, J. Phys. A **19**, 2041 (1986).
[35] P. Descouvemont, C. Daniel, and D. Baye, Phys. Rev. C **67**, 044309 (2003).
[36] P. Descouvemont, E. Tursunov, and D. Baye, Nucl. Phys. **A765**, 370 (2006).
[37] J. S. Al-Khalili, I. J. Thompson, and J. A. Tostevin, Nucl. Phys. **A581**, 331 (1995).
[38] J. S. Al-Khalili, M. D. Cortina-Gil, P. Roussel-Chomaz, N. Alamanos, J. Barrette, W. Mittig, F. Auger, Y. Blumenfeld, J. M. Casandjian, M. Chartier *et al*., Phys. Lett. **B378**, 45 (1996).
[39] B. Abu-Ibrahim and Y. Suzuki, Nucl. Phys. **A728**, 118 (2003).
[40] J. Raynal and J. Revai, Nuovo Cimento A **68**, 612 (1970).
[41] A. M. Lane and R. G. Thomas, Rev. Mod. Phys. **30**, 257 (1958).
[42] M. Hesse, J.-M. Sparenberg, F. Van Raemdonck, and D. Baye, Nucl. Phys. **A640**, 37 (1998).
[43] M. Hesse, J. Roland, and D. Baye, Nucl. Phys. **A709**, 184 (2002).
[44] D. Baye, M. Hesse, J.-M. Sparenberg, and M. Vincke, J. Phys. B **31**, 3439 (1998).
[45] I. J. Thompson, B. V. Danilin, V. D. Efros, J. S. Vaagen, J. M. Bang, and M. V. Zhukov, Phys. Rev. C **61**, 024318 (2000).
[46] M. Abramowitz and I. A. Stegun, *Handbook of Mathematical Functions* (Dover, London, 1970).
[47] B. V. Danilin, J. S. Vaagen, T. Rogde, S. N. Ershov, I. J. Thompson, and M. V. Zhukov, Phys. Rev. C **73**, 054002 (2006).
[48] D. R. Tilley, C. M. Cheves, J. L. Godwin, G. M. Hale, H. M. Hofmann, J. H. Kelley, C. G. Sheua, and H. R. Weller, Nucl. Phys. **A708**, 3 (2002).
[49] H. Kanada, T. Kaneko, S. Nagata, and M. Nomoto, Prog. Theor. Phys. **61**, 1327 (1979).
[50] D. Baye, Phys. Rev. Lett. **58**, 2738 (1987); J. Phys. A **20**, 5529 (1987).
[51] D. R. Thompson, M. LeMere, and Y. C. Tang, Nucl. Phys. **A286**, 53 (1977).
[52] W. Horiuchi and Y. Suzuki, Phys. Rev. C **76**, 024311 (2007).
[53] V. I. Kukulin and V. M. Krasnopol'sky, J. Phys. A **10**, 33 (1977).
[54] B. Bonin, N. Alamanos, B. Berthier, G. Bruge, H. Faraggi, J. C. Lugol, W. Mittig, L. Papineau, A. I. Yavin, and J. Arvieux, Nucl. Phys. **A445**, 381 (1985).
[55] A. J. Koning and J. P. Delaroche, Nucl. Phys. **A713**, 231 (2003).
[56] I. J. Thompson, F. M. Nunes, and B. V. Danilin, Comput. Phys. Commun. **161**, 87 (2004).
[57] G. Hagen, M. Hjorth-Jensen, and J. S. Vaagen, Phys. Rev. C **71**, 044314 (2005).
[58] T. Nakamura, A. M. Vinodkumar, T. Sugimoto, N. Aoi, H. Baba, D. Bazin, N. Fukuda, T. Gomi, H. Hasegawa, N. Imai *et al*., Phys. Rev. Lett. **96**, 252502 (2006).
[59] P. Capel, G. Goldstein, and D. Baye, Phys. Rev. C **70**, 064605 (2004).
[60] T. Sugimoto, T. Nakamura, Y. Kondo, N. Aoi, H. Baba, D. Bazin, N. Fukuda, T. Gomi, H. Hasegawa, N. Imai *et al*., Phys. Lett. **B654**, 160 (2007).